Physics – Uspekhi **49** (6) 605 – 628 (2006)

REVIEWS OF TOPICAL PROBLEMS PACS numbers: 42.65.Dr, 42.65.Ky, 42.65.Re, 42.65.Wi

Let there be white light: supercontinuum generation by ultrashort laser pulses

A M Zheltikov

DOI: 10.1070/PU2006v049n06ABEH005975

Contents

Abstract. Three centuries after Newton's experiments on the decomposition of white light into its spectral components and the synthesis of white light from various colors, nonlinear-optical transformations of ultrashort laser pulses have made it possible to produce an artificial white light with unique spectral properties, controlled time duration, and a high spectral brightness. Owing to its broad and continuous spectrum, such radiation is called supercontinuum. The laser generation of white light is an interesting physical phenomenon and the relevant technology is gaining in practical implications — it offers novel solutions for optical communications and control of ultrashort laser pulses, helps to achieve an unprecedented precision in optical metrology, serves to probe the atmosphere of the Earth, and suggests new strategies for the creation of compact multiplex light sources for nonlinear spectroscopy, microscopy, and laser biomedicine. Here, we provide a review of physical mechanisms behind the laser generation of white light, examine its applications, and discuss the methods of generation of broadband radiation with controlled spectral, temporal, and phase parameters.

A.M. Zheltikov Physics Department, International Laser Center, M V Lomonosov Moscow State University, Vorob'evy gory, 119992 Moscow, Russian Federation
Tel. (7-495) 939 51 74. Fax (7-495) 939 31 13
E-mail: zheltikov@phys.msu.ru

Received 9 December 2005
Uspekhi Fizicheskikh Nauk **176** (6) 623 – 649 (2006)
Translated by A M Zheltikov; edited by A Radzig

1. Introduction

Over many centuries, white light coming from the Sun served as a key tool in experimental optics. Studies performed either directly with sunlight or with objects illuminated by sunlight have led to the discovery of many laws of geometrical optics, including the laws of refraction and reflection of light, clarified the geometric-optical aspects of vision and image formation in optical systems, and allowed observation of a variety of fundamental optical phenomena.

Until the middle of the 17th century, however, physics did not relate sunlight with the amazing wealth of colors perceived in the most striking way in the light of the day. Light had no color. Important milestones on the way toward the development of the physico-physiological concept of color perception included the explanation of a rainbow by Descartes [1] and the work by Grimaldi [2] who observed the appearance of color rings around a spot of sunlight penetrating a nontransparent screen with a small pinhole. Newton's experiments on the refraction of sunlight rays by a prism and synthesis of white light by another, crossed prism [3] were the first to demonstrate the presence of colors in the sunlight itself (see Fig. 1a). Newton's discovery of the nature of colors was reported in 1672. White light turned out to be a mixture of the whole palette of colors rather than an elementary form of radiation borrowing its color from objects it illuminated or shined through, as was believed before Newton.

In 1928, Raman and Krishnan used sunlight as a radiation source for the observation of what they called a new type of secondary scattering [4], or modified red-shifted scattered radiation, in liquids and gases exposed to the action of sunlight. In-depth studies of this phenomenon [5 – 7] (see also Ref. [8] for a review), called Raman scattering, have

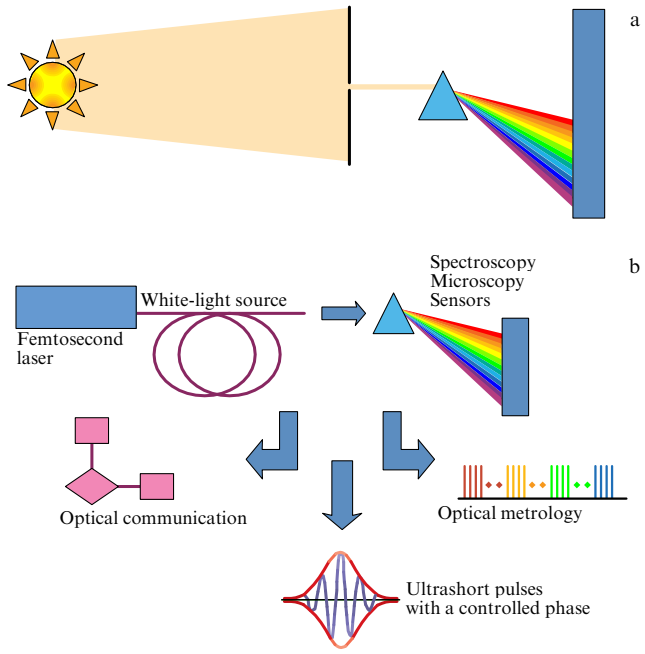

Figure 1. (a) Decomposition of white light coming from the Sun into its spectral components in Newton's experiments. (b) The main applications of the white light generated through nonlinear-optical transformations of ultrashort laser pulses.

revealed the physical nature of the frequency shift accompanying the light scattering from molecules and have shown that this inelastic scattering of light offers unique options for spectroscopic studies of the condensed and gas phases of matter. For the discovery of this effect, Raman was awarded the Nobel Prize in Physics 1930.

Seventy five years later, a part of the Nobel Prize in Physics 2005 was awarded to Theodor Hänsch and John Hall for their work on "laser-based precision spectroscopy, including the optical frequency comb technique" [9]. Fiber structures providing a transformation of ultrashort laser pulses into a broadband supercontinuum radiation (artificial white light) have been figuratively called by Hänsch a missing link in the femtosecond clockwork — a unique device of high-precision optical metrology.

Revolutionary achievements in laser spectroscopy, as well as impressive progress in recent years in ultrafast science, nonlinear and quantum optics, and laser biomedicine, are largely based on the laser generation of artificial white light, the so-called supercontinuum (see Fig. 1b). Three centuries after Newton's experiments on the decomposition of white light into its spectral components (Fig. 1a) and synthesis of white light from a variety of colors, nonlinear-optical transformations of ultrashort laser pulses have made it possible to generate an artificial white light with unique spectral properties, a controlled pulse width, and high spectral brightness (Fig. 1b). The spectrum of the supercontinuum can stretch over the entire visible and part of the near-infrared regions. The spectral brightness and intensity of laser-induced white light are millions of times higher than those of the natural white light coming to the Earth from the Sun. The physical mechanisms behind the laser generation of white light and the methods allowing a control of the spectral, temporal, and phase parameters of supercontinuum radiation are the main subjects of this review.

2. Discovery of and early studies in supercontinuum generation

The generation of white light by laser radiation was first reported by Alfano and Shapiro [10] who observed a spectral broadening of a picosecond second-harmonic output of a neodymium garnet laser with an energy of about 5 mJ in the bulk of borosilicate glass. With the intensity of laser pulses in the sample, being on the order of 1 GW cm^{-2}, the spectrum of laser pulses transmitted through the sample stretched from 400 to 700 nm. These findings, as well as the communication [11] of the same authors, reporting supercontinuum generation accompanied by the formation of thin laser radiation filaments in calcite, quartz, sodium chloride, and various types of glass, were published in 1970, i.e., about 300 years after the publication of the results of the prism experiments by Newton.

Experimental studies in supercontinuum generation, initiated by the Alfano and Shapiro publications, have demonstrated that the supercontinuum can be generated in materials of different nature and structure, including solid-state materials [12], organic and inorganic liquids [13 – 16], and gas media [17, 18]. Experiments performed with bulk samples were followed by studies on waveguide white-light generation in silica optical fibers [19, 20]. Research in laser white-light generation in the 1970s and 1980s has facilitated the creation of novel broadband light sources for spectroscopy and time-resolved measurements [19]. These studies have also given powerful momentum to the development of the theory of temporal and spatial self-action of ultrashort laser pulses [17, 21]. Starting with the late 1980s, supercontinuum generation has also been employed for the formation of ultrashort light pulses [22 – 24] and the creation of multifrequency multiplex light sources [25]. An illuminating overview of the early phase of experimental and theoretical studies of supercontinuum generation in the 1970s and 1980s can be found in the classical book edited by Alfano [26]. In this review, we choose not to provide a detailed discussion of the early-stage results on supercontinuum generation, which have been systematically and thoughtfully presented in Ref. [26]. Instead, we will focus on the achievements of the past 5 – 7 years. Within this period, the advent of novel waveguide structures and progress in laser sources have made it possible [27] to apply supercontinuum generation to solving a broad class of fundamental and applied problems in ultrafast science, nonlinear spectroscopy and microscopy, laser biomedicine, and remote sensing of the terrestrial atmosphere. Supercontinuum generation has also been at the heart of the revolutionary breakthrough in optical metrology.

3. Self-phase modulation and the elementary theory of spectral broadening of ultrashort laser pulses

The Kerr-nonlinearity-induced intensity-dependent additive to the refractive index is one of the key physical factors in supercontinuum generation. The refractive index of a medium with a Kerr nonlinearity is written as [28]

$$n = n_0 + n_2 I(t)\,, \tag{1}$$

where n_0 is the field-free nonperturbed refractive index of the medium, $n_2 = (2\pi/n_0)^2 \chi^{(3)}(\omega;\omega,\omega,-\omega)$ is the nonlinear

refractive index at the frequency ω, $\chi^{(3)}(\omega;\omega,\omega,-\omega)$ is the third-order nonlinear-optical susceptibility, and $I(t)$ is the laser radiation intensity.

In the case of short laser pulses, the intensity-dependent additive to the refractive index gives rise to a physically significant phase modulation of the laser field, the so-called self-phase modulation (SPM).

We use formula (1) to represent the nonlinear phase incursion acquired by a laser pulse over a distance L in a medium with a Kerr nonlinearity in the form

$$\Phi(t) = \frac{\omega}{c}\, n_2 I(t) L\,. \tag{2}$$

It can be seen from expression (2) that the intensity dependence of the refractive index of the medium maps the temporal profile of the field intensity in a laser pulse on the time dependence of the nonlinear phase shift, which, in turn, gives rise to a time-dependent frequency deviation across the laser pulse:

$$\Delta\omega(t) = \frac{\omega}{c}\, n_2 L\, \frac{\partial I}{\partial t}\,. \tag{3}$$

The maximum SPM-induced spectral broadening of the laser pulse can then be estimated as

$$\Delta\omega = \frac{\omega}{c}\, n_2 L\, \frac{I_0}{\tau}\,, \tag{4}$$

where I_0 is the peak intensity of the laser pulse, and τ is the pulse width.

More accurate expressions for the temporal envelope of the laser pulse and the SPM-induced phase shift can be derived with the use of an elementary theory of SPM, based on the slowly varying amplitude approximation and the first-order series expansion of the propagation constant $\beta(\omega)$ [or the wave number $k(\omega)$ for light pulses in the bulk of a nonlinear material]:

$$\beta(\omega) \approx \beta(\omega_0) + u^{-1}(\omega - \omega_0)\,,$$

where ω_0 is the central frequency of the light pulse, and $u = (\partial\beta/\partial\omega|_{\omega=\omega_0})^{-1}$ is its group velocity. In this approximation, the equation governing the evolution of the slowly varying envelope $A(t,z)$ of the laser pulse is written in the form [28, 29]

$$\frac{\partial A}{\partial z} + \frac{1}{u}\,\frac{\partial A}{\partial t} = \mathrm{i}\tilde{\gamma}|A|^2 A\,, \tag{5}$$

where $\tilde{\gamma}$ is the nonlinear coefficient equal to

$$\tilde{\gamma} = \frac{3\pi\omega}{2n_0^2 c}\,\chi^{(3)}(\omega;\omega,-\omega,\omega)\,. \tag{6}$$

In the retarded frame of reference with $z' = z$ and $\eta = t - z/u$, the solution to Eqn (5) is represented as

$$A(\eta,z) = A_0(\eta)\exp\left[\mathrm{i}\tilde{\gamma}\left|A_0(\eta)\right|^2 z\right], \tag{7}$$

where $A_0(\eta)$ is the initial pulse envelope.

Since the second- and higher-order dispersion effects have been ignored in Eqn (5), the solution given by formula (7) predicts no changes in the envelope of the laser pulse. The evolution of the nonlinear phase shift in this regime is governed by the expression

$$\varphi_{\mathrm{nl}}(\eta,z) = \gamma_{\mathrm{SPM}} I_0(\eta) z\,, \tag{8}$$

where $\gamma_{\mathrm{SPM}} = 2\pi n_2/\lambda$, and $I_0(\eta)$ is the intensity envelope of the laser pulse.

The deviation of the instantaneous frequency of the laser field from the central frequency ω_0 is then given by

$$\delta\omega(\eta,z) = -\frac{\partial\varphi_{\mathrm{nl}}(\eta,z)}{\partial t} = -\gamma_{\mathrm{SPM}}\,\frac{\partial I_0(\eta)}{\partial\eta}\,z\,. \tag{9}$$

For a laser pulse with a quadratic dependence of the intensity envelope on the retarded time, viz.

$$I_0(\eta) \approx I_0(0)\left(1 - \frac{\eta^2}{\tau_0^2}\right)$$

(notably, such an approximation is valid near the peak of an arbitrary laser pulse), the SPM induces a linear chirp:

$$\delta\omega(\eta,z) \approx 2\gamma_{\mathrm{SPM}}\,\frac{I_0(0)}{\tau_0^2}\,\eta z\,. \tag{10}$$

Such a chirp can be conveniently compensated by using a set of prisms, diffraction gratings, or chirped mirrors [30], allowing a temporal compression of the laser pulse.

The spectrum of the phase-modulated pulse is given by the expression

$$S(\omega) = \left|\int_0^\infty I(\eta)\exp\left[\mathrm{i}\omega\eta + \mathrm{i}\varphi_{\mathrm{nl}}(\eta)\right]\mathrm{d}\eta\right|^2. \tag{11}$$

Within the framework of the above-described elementary theory of SPM, which includes only the first-order dispersion effects, temporal self-action induces a symmetric spectral broadening of the laser pulse (see Fig. 2). However, even for moderate laser intensities, the spectral broadening of the laser pulse may become asymmetric because of a number of physical factors. The three most significant mechanisms inducing an asymmetry in SPM-broadened spectra include spatial self-action, shock waves, and the retarded part of the

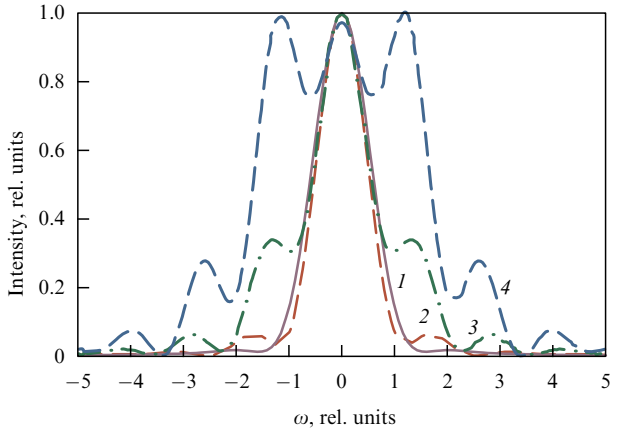

Figure 2. Self-phase-modulation-induced spectral broadening of a hyperbolic-secant-shaped laser pulse with an initial pulse width of 30 fs in a fused silica optical fiber with $n_2 = 3.2\times10^{-16}$ cm^2 W^{-1}. Curve *1* presents the input spectrum of the laser pulse. The input pulse energy is (*2*) 0.1 nJ, (*3*) 0.2 nJ, and (*4*) 0.3 nJ.

nonlinear-optical response of the medium. Below in this section, we briefly characterize each of these factors.

Spatial self-action [28, 31] is related to the Kerr nonlinearity of a medium. Similar to the temporal profile of the field-intensity envelope $I(t)$ inducing phase modulation of a pulse, the radial profile of the field intensity $I(r)$ in a laser beam causes a self-focusing or self-defocusing of a laser beam, depending on the sign of n_2, through the transverse profile of the refractive index $n(r) = n_0 + n_2 I(r)$ corresponding to a nonlinear lens. The growing radiation intensity of a self-focusing laser beam enhances nonlinear-optical interactions. Typically, self-focusing of high-power laser pulses is accompanied by noncontrolled intensity and phase variations of the laser field, launching complicated beam dynamics and making a laser beam unstable with respect to filamentation. Spectral and temporal transformations of laser pulses in filaments give rise to a broadband emission. It is, however, very difficult to precisely control the properties of such emission.

Intensity dependence of the group velocity of a laser pulse in a nonlinear medium causes the formation of shock fronts in the intensity envelope of the laser field [29, 32]. In a medium with $n_2 > 0$, the nonlinearity induces a positive additive to the group velocity. The peak of the pulse under these conditions propagates more slowly than its edges, making the trailing edge of the pulse steeper and reducing the slope of the leading edge. In the frequency domain, such a transformation of a laser pulse manifests itself in an asymmetry of its spectrum. With $n_2 > 0$, the maximum of the intensity spectrum displays a noticeable red shift, with the blue wing of the spectrum becoming much more extended than its red wing.

Effects related to the retarded nonlinearity become especially pronounced for short laser pulses, when the nonlinearity of the medium can no longer be regarded as instantaneous [29, 33]. Retarded nonlinearity in the time domain is equivalent to the dispersion of nonlinearity in the frequency representation, resulting in a red shift of the spectrum of an ultrashort laser pulse. The spectral transformation of an ultrashort laser pulse, induced by a retarded nonlinearity, is thus equivalent to the Raman effect. A more detailed discussion of retarded optical nonlinearity and its role in supercontinuum generation will be provided in Section 6.2 of this review.

4. Supercontinuum generation by high-intensity laser pulses

Supercontinuum generation by high-intensity femtosecond laser pulses in gas and liquid media [34–48] constitutes an interesting and practically significant scenario of nonlinear-optical short-pulse transformation. The peak powers of laser pulses used for such experiments typically fall within the terawatt range. High-intensity laser radiation ionizes a medium, generating free electrons which contribute to the nonlinear response of a medium, modifying the spectral, temporal, and spatial dynamics of laser pulses. In particular, the filamentation phenomenon [37–45] observed for high-intensity laser pulses propagating in gas media allows supercontinuum generation to be employed for the remote sensing of the Earth's atmosphere [46–48].

Along with ionization effects, supercontinuum generation by high-intensity laser pulses involves spatial self-action, shock-front formation in the intensity envelope, retarded nonlinearity of the medium, and high-order dispersion effects. All these phenomena are included in the following equation for the slowly evolving field amplitude A normalized to the peak field amplitude [49, 50]:

$$\left[\mathrm{i}\frac{\partial}{\partial z}+\frac{1}{4}\left(1-\mathrm{i}s\frac{\partial}{\partial\tau}\right)\nabla_\perp^2-\frac{1}{4}\frac{L_{\mathrm{df}}}{L_{\mathrm{d}}}\left(\frac{\partial^2}{\partial\tau^2}+\frac{\mathrm{i}}{3}\frac{L_{\mathrm{d}}}{L'_{\mathrm{d}}}\frac{\partial^3}{\partial\tau^3}\right)\right]A + L_{\mathrm{df}}\left(1+\mathrm{i}s\frac{\partial}{\partial\tau}\right)\left(\frac{\Psi_{\mathrm{nl}}}{L_{\mathrm{nl}}}-\frac{|A|^4}{L_{\mathrm{s}}}\right)A - \frac{L_{\mathrm{df}}}{L_{\mathrm{pl}}}\left(1-\mathrm{i}s\frac{\partial}{\partial\tau}\right)N_{\mathrm{e}}A+\mathrm{i}\frac{L_{\mathrm{df}}}{L_{\mathrm{MPA}}}|A|^{2n-2}A=0\,, \quad (12)$$

where $s=(\omega\tau_0)^{-1}$, τ_0 is the initial pulse width, $\tau = t - z/u$ is the retarded time, $u=(\partial k/\partial\omega)^{-1}$ is the group velocity of the laser pulse, and $k=\omega n_0/c$. The function Ψ_{nl} includes both the instantaneous and retarded parts of optical nonlinearity:

$$\Psi_{\mathrm{nl}} = (1-f_{\mathrm{R}})\,|A|^2 + f_{\mathrm{R}}\int_{-\infty}^{\tau} R(\tau-\theta)\,|A(\theta)|^2\,\mathrm{d}\theta\,, \quad (13)$$

where $R(\eta)$ is the Raman response function related to the retarded part of optical nonlinearity, and f_{R} is the fraction of the Raman nonlinearity in the overall Kerr nonlinearity of the medium.

Equation (12) comprises the following spatial scales [49, 50]. The diffraction length is defined as $L_{\mathrm{df}} = kw_0^2/2$, where w_0 is the radius of the laser beam. Dispersion effects are quantified in terms of length scales where the second- and third-order dispersion becomes noticeable, $L_{\mathrm{d}} = \tau_0^2(2k_2)^{-1}$ and $L'_{\mathrm{d}} = \tau_0^3(2k_3)^{-1}$, where $k_2 = \partial^2 k/\partial\omega^2$ and $k_3 = \partial^3 k/\partial\omega^3$. The nonlinear interaction length $L_{\mathrm{nl}} = c(\omega n_2 n_0 I_0)^{-1}$ is controlled by the nonlinear refractive index n_2 and the laser peak intensity I_0. The fifth-order nonlinearity tends to arrest (saturate) self-focusing within the characteristic length $L_{\mathrm{s}} = c(\omega n_4 n_0 I_0^2)^{-1}$, where n_4 is determined by the fifth-order nonlinear susceptibility $\chi^{(5)}$. The parameters $L_{\mathrm{pl}} = km_{\mathrm{e}}c^2(2\pi e^2\tau_0 N_0\sigma^{(n)}I_0^n)^{-1}$ and $L_{\mathrm{MPA}} = n\hbar\omega N_0\sigma^{(n)}I_0^{n-1}/2$ define the spatial scales where plasma formation and multiphoton absorption related to ionization loss come into play. Here, m_{e} and e are the mass and the charge of an electron, N_0 is the number density of neutral species, and $\sigma^{(n)}$ is the cross section of n-photon ionization. The electron number density N_{e} in Eqn (12) is normalized to the parameter $\tau_0 N_0\sigma^{(n)}I_0^n$. For the atmosphere of the Earth under normal conditions and a laser-radiation central wavelength equal to 800 nm, the main medium parameters appearing in Eqn (12) are estimated as $N_0 \approx 3\times10^{19}\ \mathrm{cm}^{-3}$, $k_2 \approx 0.2\ \mathrm{fs}^2\ \mathrm{cm}^{-1}$, $k_3 \approx 0.1\ \mathrm{fs}^3\ \mathrm{cm}^{-1}$, and $n_2 \approx 4\times10^{-19}\ \mathrm{cm}^2\ \mathrm{W}^{-1}$. The Raman response function related to Raman-active modes of molecules is modelled as a response of a damped oscillator [43, 51]:

$$R(\eta) \propto \Theta(\eta)\exp\left(-\frac{\eta}{\tau_1}\right)\sin\left(\frac{\eta}{\tau_2}\right), \quad (14)$$

where $\Theta(\eta)$ is the Heaviside step function. For the Earth's atmosphere, $\tau_1 \approx 77$ fs and $\tau_2 \approx 62.5$ fs.

In the absence of the terms describing ionization and plasma effects, as well as spatial self-action, equation (12) is reduced to the generalized Schrödinger equation [52] for the field envelope in a medium with a cubic dispersion profile (see Section 6.2 of this review). Analysis of the propagation of high-intensity ultrashort laser pulses in the atmosphere using Eqn (12) was performed in Refs [45, 49, 50].

Both numerical analysis and experimental investigations demonstrate that nonlinear-optical transformations of high-intensity laser pulses in the atmosphere allow the generation of high-energy supercontinuum radiation. The spectrum of the supercontinuum generated by high-intensity laser pulses in the atmosphere (or in a liquid) features a well-pronounced peak at the pump wavelength. Although the total energy of supercontinuum radiation is typically rather high, its spectral density in the visible portion of the spectrum falls off quite rapidly with a characteristic rate of one to two orders of magnitude per 100 nm. The generation of supercontinua with more uniform and broader spectra is impeded by plasma defocusing, multiphoton absorption arresting spatial self-action [53–56], and dispersion profiles allowing no phase matching for a broad class of nonlinear-optical interactions [57]. Remote sensing of the terrestrial atmosphere is currently one of the most interesting and practically significant applications of white-light generation by high-intensity laser pulses [46, 48]. A terawatt mobile lidar complex for the remote sensing of the atmosphere was developed as a part of the European Teramobile program [48]. This system provides a collection of the lidar signal within the range of wavelengths from 1.0 to 1.7 μm, enabling the remote sensing of the atmosphere up to an altitude of 4 km.

5. Four-wave mixing and soliton mechanisms of supercontinuum generation in optical fibers

As was shown in Sections 3 and 4, white-light generation by focused laser beams is often observed in the regime of spatial self-action and is accompanied by the complicated spatial and temporal dynamics of a laser pulse. Optical fibers, on the other hand, provide longer lengths of nonlinear-optical interactions for laser pulses with a sufficiently high intensity, allowing the requirements to the input laser power necessary for efficient supercontinuum generation to be considerably loosened. The intensity of supercontinuum radiation generated in optical fibers is typically lower than the intensity of white light produced by high-power focused laser pulses in gas media (see Section 4). As a generous payoff, however, optical fibers enable the generation of supercontinua whose spectra span the entire visible and a considerable part of the near-infrared spectral regions [19] even with input peak powers as low as 1 kW. Optical fiber technologies, as will be shown in Sections 6 and 7 of this review, offer vast opportunities for controlled white-light generation with tailored spectral and temporal parameters of the supercontinuum fiber output.

As shown by early experiments on supercontinuum generation in optical fibers [19, 20], performed with the use of pico- and nanosecond laser pulses, new components are efficiently generated in the spectrum of a light pulse propagating through a fiber due to cascaded stimulated Raman scattering (SRS) and parametric four-wave mixing (FWM). New spectral components originating from these processes then broaden through self- and cross-phase modulation, merging together and giving rise to a radiation with a continuous broadband spectrum at the output of the fiber.

Four-wave mixing in optical fibers [26] involves a parametric conversion of pump fields with frequencies ω_{p1} and ω_{p2} into light fields with frequencies ω_a and ω_s. This process becomes especially efficient when the FWM energy conservation law, $\omega_{p1} + \omega_{p2} = \omega_a + \omega_s$, is obeyed jointly with momentum conservation law (also known in nonlinear optics as phase matching), $\beta_{p1} + \beta_{p2} = \beta_a + \beta_s$, where β_{p1}, β_{p2}, β_a, and β_s are the propagation constants of the guided modes with frequencies ω_{p1}, ω_{p2}, ω_a, and ω_s involved in the FWM process. For a pump-frequency-degenerate FWM, with $\omega_{p1} = \omega_{p2} = \omega_p$, $\omega_a = \omega_p + \Omega$, and $\omega_s = \omega_p - \Omega$, the phase-matching condition

$$2\beta(\omega_p) = \beta(\omega_p - \Omega) + \beta(\omega_p + \Omega) \tag{15}$$

is automatically satisfied in the range of anomalous group-velocity dispersion (GVD) near the wavelength of zero GVD. To illustrate this important result, we represent the propagation constants at the Stokes and anti-Stokes frequencies ω_s and ω_a as power series:

$$\beta(\omega_s) \approx \beta_0(\omega_p) - \frac{1}{u_p}\,\Omega + \frac{1}{2}\,\beta_2(\omega_p)\,\Omega^2 + 2\gamma P\,, \tag{16}$$

$$\beta(\omega_a) \approx \beta_0(\omega_p) + \frac{1}{u_p}\,\Omega + \frac{1}{2}\,\beta_2(\omega_p)\,\Omega^2 + 2\gamma P\,, \tag{17}$$

where P is the peak power of the pump pulse, $\beta_0(\omega_p)$ is the propagation constant of the waveguide mode at the pump frequency in the absence of the field-induced additive to the refractive index (i.e., with $P = 0$), $u_p = (\partial\beta/\partial\omega|_{\omega=\omega_p})^{-1}$ is the group velocity of the pump pulse, $\beta_2(\omega_p) = \partial^2\beta/\partial\omega^2|_{\omega=\omega_p}$,

$$\gamma = \frac{n_2\omega_p}{cS_{\text{eff}}} \tag{18}$$

is the nonlinear coefficient, and

$$S_{\text{eff}} = \frac{\left[\int_{-\infty}^{\infty}\int_{-\infty}^{\infty}\left|F(x,y)\right|^2 \mathrm{d}x\,\mathrm{d}y\right]^2}{\int_{-\infty}^{\infty}\int_{-\infty}^{\infty}\left|F(x,y)\right|^4 \mathrm{d}x\,\mathrm{d}y}$$

is the effective area of a guided mode with a transverse field profile $F(x, y)$.

With the propagation constant of the pump field represented as

$$\beta(\omega_p) = \beta_0(\omega_p) + \gamma P\,, \tag{19}$$

the phase-matching condition (15) gives

$$\beta_2(\omega_p)\,\Omega^2 + 2\gamma P = 0\,. \tag{20}$$

The requirement of Eqn (20) can be fulfilled only for $\beta_2(\omega_p) < 0$, i.e., in the anomalous dispersion region. These simple arguments explain why supercontinuum radiation sources based on standard optical fibers are usually especially efficient with a near-infrared pump field and are much less efficient in generating a frequency-shifted output in the visible portion of the spectrum [19]. Indeed, the zero-GVD wavelength of standard optical fibers is typically close to $\lambda_z \approx 1.3$ μm. The frequency region where the phase-matching condition (15) is satisfied is then limited to a quite narrow spectral interval in the near-infrared range. Another mechanism of supercontinuum generation in standard optical fibers involves SRS. In this regime, the spectrum of the laser field experiences a predominant red (Stokes) shifting. In standard optical fibers, however, SRS does not lead to efficient frequency conversion to the visible portion of the spectrum.

Supercontinuum generation in optical fibers offers interesting strategies for the development of multifrequency radiation sources for wavelength multiplexing in fiber-optic communication lines. This class of applications requires a

highly efficient frequency conversion of gigahertz light pulses with the generation of broadband radiation with a flat spectrum and a low level of noise at the output of the fiber. One of the promising solutions to this problem involves an adiabatic compression of solitons in the regime of anomalous dispersion in fibers with a longitudinally varying GVD [58]. Another class of solutions is based on the spectral broadening of laser pulses through SPM in the regime of normal dispersion [32] in fibers with low GVD values and specifically tailored, flattened dispersion profiles, designed to reduce dispersion spreading of light pulses. A combination of the above-described approaches, as shown in Ref. [59], allows the creation of a 10-Gbit s^{-1} supercontinuum fiber-optic source.

Fibers of a novel type — photonic-crystal fibers (PCFs) [60 – 62] — can serve as fiber-optic sources of supercontinuum radiation with a spectrum stretching over the entire visible and near-infrared spectral regions. The main physical mechanisms and scenarios of supercontinuum generation in these fibers are examined in Section 6 of this review.

6. Laser generation of white light in photonic-crystal fibers

6.1 Photonic-crystal fibers: tailoring dispersion and nonlinearity

Photonic-crystal fibers [60 – 62], also referred to as microstructure (or holey) fibers, constitute waveguide structures of a novel type. In contrast to conventional optical fibers consisting of a core with the refractive index $n_{\rm core}$ and a cladding with the refractive index $n_{\rm clad}$, PCFs guide electromagnetic radiation through a fused silica or multicomponent-glass microstructure with a periodic or aperiodic array of air holes running along the fiber axis (Fig. 3). Fabrication of such a microstructure typically involves drawing a preform consisting of an array of capillaries at a high temperature. A defect in this microstructure, formed by one or several missing air holes (at the center of the structure in Figs 3a – 3e), may guide the light similarly to the core in a standard fiber. In conventional fibers, the light is confined to the fiber core by total internal reflection, provided that the inequality $n_{\rm clad} < n_{\rm core}$ is satisfied. Guided modes of electromagnetic radiation in PCFs originate from the interference of waves scattered and reflected from microinhomogeneities of the refractive index profile. For a broad class of PCFs, the condition for the existence of guided modes confined to the fiber core formed by a defect of a microstructure (Figs 3a – 3e) can be written in a form similar to the condition of total internal reflection in a conventional fiber, viz. $\bar{n}_{\rm clad} < n_{\rm core}$, where $\bar{n}_{\rm clad} = \beta_{\rm f} c/\omega$ is the effective refractive index of the microstructure cladding, defined through the propagation constant $\beta_{\rm f}$ of the fundamental space-filling mode of the cladding [63, 64].

Along with conventional waveguiding regimes supported by total internal reflection, PCFs can under certain conditions guide electromagnetic radiation due to the high reflectivity of the fiber cladding within photonic band gaps [65 – 68]. Such regimes of waveguiding can be implemented in fibers with a two-dimensionally periodic microstructure cladding (a two-dimensional photonic crystal) and a hollow core (Fig. 3f). Photonic band gaps arising in the transmission spectrum of a two-dimensionally periodic cladding in fibers of this type provide high reflection coefficients for radiation propagating along the hollow core, radically reducing optical losses which are typical of air-guided modes in conventional hollow fibers and which rapidly grow with a decrease in the core diameter of a hollow fiber [69, 70].

The unique properties of PCFs open up new routes for a long-distance transmission of electromagnetic radiation [60], as well as for nonlinear-optical transformation of laser pulses [71, 72]. As shown by Knight et al. [63], PCFs can support single-mode waveguiding within a remarkably broad frequency range. Photonic-crystal fibers offer new solutions for laser physics, nonlinear optics, and optical technologies, as they combine dispersion tunability and a high degree of light-field confinement in the fiber core. Dispersion of such fibers is

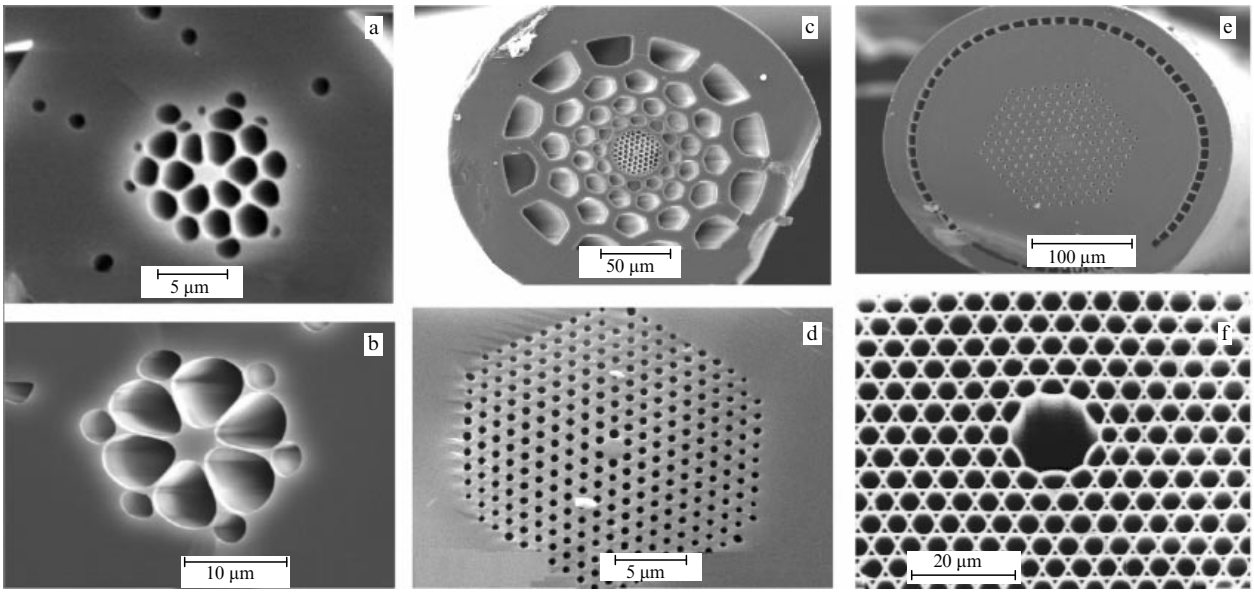

Figure 3. Cross-section images of photonic-crystal fibers: (a, b) PCFs with a high air-filling fraction of the cladding, (c) PCF with a double microstructure cladding, (d) PCF with a periodic cladding, (e) PCF with a doped core and a double microstructure cladding, and (f) hollow-core PCF with a photonic band-gap cladding.

tailored by changing their core–cladding geometry [73, 74], while a strong light-field confinement is due to the high refractive-index step between the core and the microstructure cladding [75]. Controlled dispersion of PCFs paves the way to new solutions in optical telecommunications and ultrafast photonics. The high degree of light-field confinement, on the other hand, radically enhances the whole catalogue of nonlinear-optical processes and allows observation of new nonlinear-optical phenomena.

Several classes of PCFs have been developed to meet the demands of fundamental science and applied research, including the solution of specific problems in nonlinear optics, optical metrology, laser physics, and biomedical optics [60, 62, 64]. Figures 3a and 3b display the sectional views of PCFs with a high refractive-index step from the fiber core to the fiber cladding, controlled by the air-filling fraction of the microstructure cladding. Fibers of this type can strongly confine electromagnetic radiation in the fiber core, providing high values of nonlinearity coefficient γ [see formula (18)] controlling the efficiency of nonlinear-optical interactions. Therefore, such fibers are often referred to as highly nonlinear PCFs. Enhanced nonlinearity and controlled dispersion of guided modes allow controlled supercontinuum generation (Fig. 4a) using low-energy laser fields, including unamplified femtosecond pulses [76, 77]. Supercontinua with spectra spanning over several octaves can often be produced with such fibers. Supercontinuum-generating PCFs lead to revolutionary changes in optical metrology [78–81] and are widely employed in laser biomedicine [82], nonlinear spectroscopy [83, 84] and microscopy [85], photochemistry [86], quantum optics [87, 88], and ultrafast optics [89].

Dispersion control of guided modes helps to phase-match FWM processes in PCFs [90–92], allowing these fibers to be employed not only as sources of broadband emission, but also as efficient frequency converters for ultrashort laser pulses [72, 93]. The size of the waveguiding channel in a PCF is the key parameter governing the dispersion properties of guided modes. Arrays of submicron fused silica threadlike channels that are microstructure-integrated into PCFs can, therefore, function as multiplex frequency upconverters (Figs 4b, 4c), providing high efficiencies of nonlinear-optical spectral transformation even in the case of nano- and subnanojoule ultrashort laser pulses [72].

The PCFs shown in Fig. 3b exhibit a strong form anisotropy related to the ellipticity of the fiber core. Form anisotropy induces a strong birefringence in such fibers. As a result, orthogonal-polarized modes with nearly identical spatial profiles of field intensity can substantially differ in their propagation constants, mode indices, group velocities, GVDs, and other parameters. PCF architecture provides an opportunity [94–96] to create fibers with a very high birefringence $\delta n = |n_x - n_y|$, where n_x and n_y are the mode indices of fiber modes with orthogonal polarizations. Birefringent PCFs allow efficient polarization control of nonlinear phenomena, including supercontinuum generation [97, 98] and radiation wavelength conversion [99, 100], suggesting ways of creating polarization-demultiplexed supercontinuum sources [101] through a polarization separation of orthogonal-polarized broadband emission bands at the output of the fiber.

Photonic-crystal fibers with a dual cladding (Figs 3c, 3e) are of special interest for the creation of fiber-optic lasers and amplifiers [102, 103], as well as the development of novel optical sensors [104–106]. In PCF lasers, the inner part of the microstructure cladding provides single-mode guiding within a large mode area, allowing the generation of high output powers. The outer part of the cladding confines pump radiation within the inner part of the fiber. In PCF sensors, exciting radiation is delivered to an object through the fiber core. The inner part of the microstructure cladding serves to deliver the scattered or fluorescence signal in the backward direction toward a detector which can be thus located adjacent to a light source [105]. The excellent performance of such a fiber design has been demonstrated in experiments where chemical and biological species were detected in solutions by means of one- and two-photon luminescence. The microstructure cladding in such fibers can also function as an array of microcapillaries filled with an ultralow volume of an analyte. Radiation propagating along the fiber core then induces a luminescence of analyte species, permitting

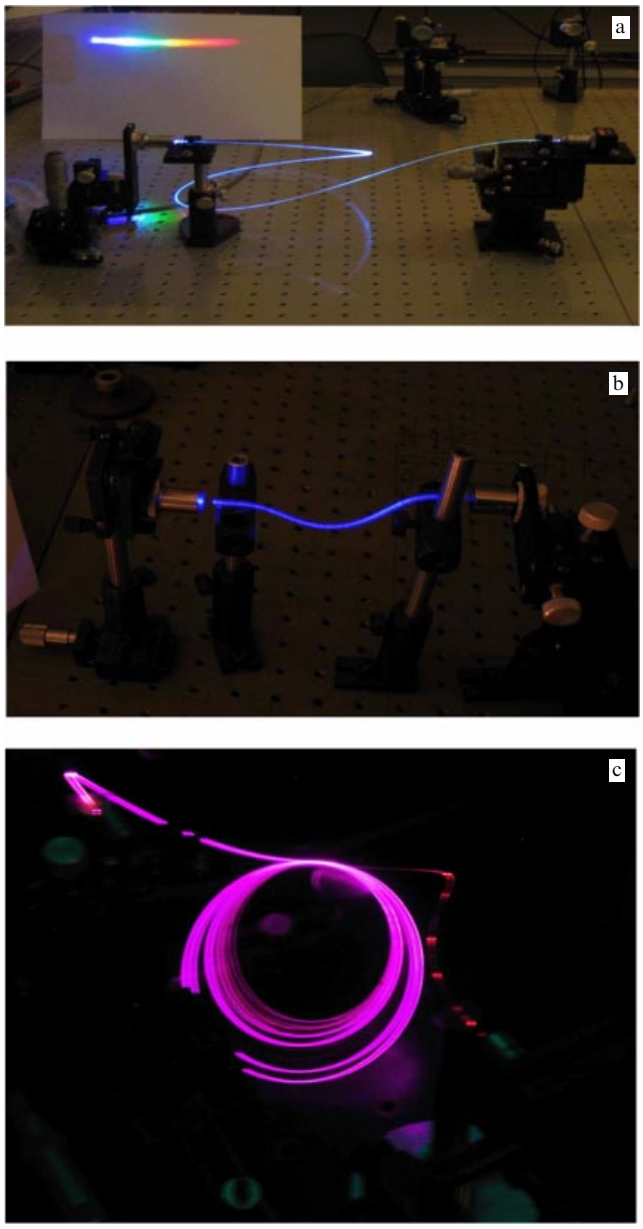

Figure 4. (a) Supercontinuum generation, and (b, c) multiplex frequency conversion in photonic-crystal fibers.

their detection [106]. Therefore, PCF sensors can be easily integrated into the databases, libraries, and processors of chemical and biological information, including biochips enabling the readout and transformation of the stored data.

Air holes periodically arranged in the cladding of the hollow-core PCFs shown in Fig. 3f support air-guided modes in such fibers [66 – 68]. The key property of two-dimensionally periodic structures (two-dimensional photonic crystals) is the existence of photonic band gaps in their transmission spectra and dispersion. Within these frequency ranges, the periodic structure becomes highly reflective, as the electromagnetic field cannot exist in the form of Bloch waves propagating inside the structure. Hollow PCFs offer unique possibilities for enhanced nonlinear-optical interactions in the gas phase [107, 108], as recently demonstrated by experiments on stimulated Raman scattering [107, 109], four-wave mixing [110, 111], coherent anti-Stokes Raman scattering (CARS) [112, 113], and self-phase modulation [114]. Hollow PCFs can also be employed for the creation of compressors [115], switches [116], limiters [117], and diodes [118] for high-power laser pulses. Hollow PCFs for the transportation of high-power laser radiation for material microprocessing [119, 120] and laser biomedicine [121] have recently been demonstrated. Temporal and spatial self-action of high-power laser pulses gives rise to the formation of temporal solitons [122, 123] and allows self-channeling of laser radiation [124], suggesting challenging ways of transmitting high-power ultrashort laser pulses. Hollow PCFs also offer promising fiber-technology-compatible strategies for the creation of new gas cells for the efficient frequency conversion of laser radiation and nonlinear spectroscopy [109, 125, 126].

In what follows, we will consider different types of PCFs providing highly efficient supercontinuum generation and enabling various regimes of spectral and temporal transformation of ultrashort laser pulses. We will examine the physical mechanisms behind supercontinuum generation in such fibers, analyze various scenarios of spectral broadening and wavelength conversion of laser radiation, and discuss applications of PCF white-light sources and frequency converters in nonlinear spectroscopy and microscopy, as well as in optical metrology.

6.2 Nonlinear-optical interactions of ultrashort pulses in photonic-crystal fibers

Supercontinuum generation in PCFs attracts much interest not only as a complicated physical phenomenon but also as a strategy for the creation of novel efficient fiber-optic-format broadband light sources [27, 76, 77, 127]. Some of the physical mechanisms behind the spectral broadening of laser pulses in PCFs are similar to the mechanisms leading to supercontinuum generation in the bulk of solids or gas-phase media. There are, however, several specific features and regimes that are inherent in nonlinear-optical processes in PCFs and that are never observed in the bulk of a solid-state sample, the gas phase, or conventional optical fibers. The key advantages of PCFs as white-light sources and frequency converters originate from the possibility of tailoring the dispersion profile of guided modes [74] and controlling optical nonlinearity by modifying the fiber structure [60]. Photonic-crystal fibers allow dispersion profiles inaccessible with conventional fiber technologies to be engineered. These unique dispersion properties of PCFs make it possible to observe novel nonlinear-optical phenomena, such as soliton self-frequency shift cancellation [128] and third-harmonic generation at a frequency different from thrice the frequency of the pump field [129, 130], as well as scalar [131] and vectorial [132] modulation instabilities of new types. With an appropriate design of PCF structure, the zero-GVD wavelength can be shifted to 750 – 800 nm. Fibers of this type allow the observation of interesting solitonic phenomena for femtosecond Ti:sapphire laser pulses and provide high efficiencies of nonlinear-optical frequency conversion of such pulses, including the blue shifting of unamplified femtosecond laser pulses.

The basic physical scenarios of supercontinuum generation in PCFs involve self- and cross-phase modulation, FWM, SRS, and modulation instabilities. Spectral transformation of ultrashort laser pulses in PCFs is especially efficient in the regime of anomalous dispersion, when input laser pulses tend to form solitons as they propagate through the fiber. In this regime, the retarded optical nonlinearity induces a continuous frequency down-shift of optical solitons — a phenomenon known as soliton self-frequency shift (SSFS) [133, 134]. High-order dispersion, on the other hand, forces solitons to emit dispersive waves [135, 136] which are typically blue-shifted with respect to the central frequency of the input field. Intermode phase matching can result in producing an intense signal around the third-harmonic frequency [129, 130, 137 – 143], which can enhance the short-wavelength wing of supercontinuum radiation at the output of the fiber. Since SPM, SRS, and FWM were discussed in Section 5 of this review, we will examine in greater detail below modulation instabilities, soliton phenomena, and third-harmonic generation. We will also discuss the role of these phenomena in white-light generation in PCFs.

6.2.1 Modulation instability and parametric frequency conversion of ultrashort light pulses. Modulation instabilities (MIs) manifest themselves in a broad class of nonlinear systems in physics, chemistry, and biology. Instabilities of this type modify wave processes in nonlinear dispersive media, giving rise to pulse–periodic field structures in time or space. Modulation instabilities are common in hydrodynamics [144], nonlinear optics [145], plasma physics [146], and matter experiencing Bose–Einstein condensation [147].

In nonlinear optics, MIs can transform the spectrum, temporal envelope, and spatial profile of the laser field [32, 148]. Optical fibers provide large lengths of nonlinear-optical interactions for the build-up of modulation instabilities [32, 149], resulting in high MI gains and efficient sideband generation in the spectrum of laser fields.

Modulation instability of femtosecond pulses in PCFs. An elementary regime of modulation instability of laser pulses involved in nonlinear-optical interactions in an optical fiber can be illustrated using formulas (15) and (19), which represent the phase-matching condition for parametric FWM: $2\omega_p = \omega_a + \omega_s$. According to Eqn (20), the efficiency of Stokes and anti-Stokes sideband generation is especially high when the central frequency of the pump pulse falls within the range of anomalous dispersion, i.e., $\beta_2(\omega_p) < 0$, and the frequency offset Ω meets the equality

$$\Omega = \pm\left(\frac{2\gamma P}{|\beta_2(\omega_p)|}\right)^{1/2}. \qquad (21)$$

Analysis of coupled equations for the amplitudes of the pump, Stokes, and anti-Stokes fields shows [32] that the

amplitudes of the Stokes and anti-Stokes fields exponentially grow within finite frequency bands around $\omega_p \pm \Omega$. The pump field is thus unstable under these conditions with respect to small perturbations at frequencies $\omega_p \pm \Omega$. The same result can be obtained by analyzing the stability of the steady-state solution to the nonlinear Schrödinger equation for the normalized field amplitude A:

$$\frac{\partial A}{\partial z} + \mathrm{i}\,\frac{\beta_2}{2}\,\frac{\partial^2 A}{\partial \tau^2} = \mathrm{i}\gamma |A|^2 A\,. \tag{22}$$

The steady-state solution to this equation becomes unstable [32] with respect to harmonic perturbations whose amplitudes tend to exponentially grow with a maximum gain achieved at the frequency defined by expression (21).

Modulation instabilities in PCFs enable efficient frequency conversion of laser radiation [131, 150], making PCFs efficient frequency shifters and sources of correlated photon pairs [87, 88]. Figure 5 presents a typical spectrum of laser pulses, transformed through a scalar MI in a PCF, as observed by Fedotov et al. [151]. In those experiments, unamplified 50-fs pulses of 795-nm Ti:sapphire laser radiation with a repetition rate of 10 MHz and an energy of 0.1–1.0 nJ were coupled into one of the microwaveguide channels off the central core of the PCF (see the inset to Fig. 5). The zero-GVD wavelength for the microwaveguide channel used to observe MI is estimated as $\lambda_z \approx 720$ nm, providing an anomalous GVD for the pump field. In the pump field at the output of the fiber intense Stokes and anti-Stokes sidebands are observed. With $\gamma \approx 50\ \mathrm{W^{-1}\ km^{-1}}$, $D \approx 30\ \mathrm{ps\ nm^{-1}\ km^{-1}}$, pulse energy $E \approx 0.5$ nJ, initial pulse duration $\tau \approx 50$ fs, we find $\Omega_{\max}/2\pi \approx 50$ THz from formula (21), which agrees well with the frequency shifts of the sidebands observed in the output spectra presented in Fig. 5. Experimental studies thus reveal interesting regimes of SPM-induced MI in microchannel waveguides of PCFs, which offer much promise for nonlinear-optical frequency conversion and parametric amplification of femtosecond laser pulses, as well as for the creation of efficient and compact fiber-optic sources of correlated photon pairs.

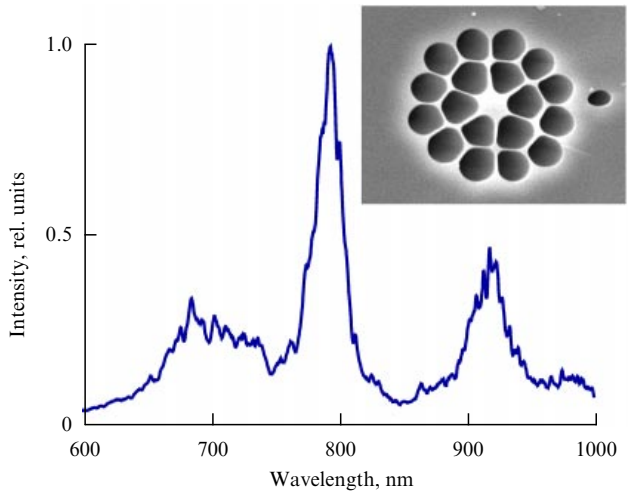

Figure 5. Sideband generation through modulation instability in the spectrum of an ultrashort laser pulse transmitted through a photonic-crystal fiber (shown in the inset). The initial pulse width is 50 fs. The input energy of the laser pulses amounts to 0.5 nJ.

Cross-phase-modulation-induced instability. As shown in the previous section, parametric frequency conversion in the regime of scalar SPM-induced modulation instability requires anomalous dispersion at the central wavelength of the pump field. This requirement, however, is no longer necessary for two-color interactions of laser pulses in the regime of modulation instabilities induced by cross-phase modulation (XPM) [32]. In particular, Serebryannikov et al. [152] presented an experimental study and theoretical analysis of XPM-induced modulation instability for a pair of spectrally resolved copropagating femtosecond laser pulses in a PCF. In this regime, the fiber serves as a highly efficient frequency converter for low-power femtosecond laser pulses. The amplitudes and the frequency shifts of the sidebands generated in the spectrum of the probe field at the output of the fiber as a result of parametric four-wave mixing are controlled by varying the intensity of the pump field.

Let us consider an XPM-induced instability for a two-color field

$$E(x,y,z,t) = F(x,y)\sum_{j=1}^{2} A_j(z,t)\exp\left[\mathrm{i}(\beta_j z - \omega_j t)\right], \tag{23}$$

where $F(x,y)$ is the transverse field profile, $A_j(z,t)$ is the temporal field envelope, β_j is the propagation constant, and ω_j is the carrier frequency of the jth pulse with $j = 1, 2$. The slowly varying envelope approximation yields the following equations for the evolution of the pump ($j = 1$) and probe ($j = 2$) pulses [153]:

$$\frac{\partial A_j}{\partial z} + \frac{1}{2}\,\alpha_j A_j + (-1)^{j-1}\delta\,\frac{\partial A_j}{\partial \tau} + \frac{\mathrm{i}}{2}\,\beta_{2j}\,\frac{\partial^2 A_j}{\partial \tau^2} = \mathrm{i}\gamma_j\left(|A_j|^2 + 2|A_{3-j}|^2\right)A_j\,, \tag{24}$$

where

$$\tau = t - \frac{z}{\bar{v}_g}\,, \qquad \bar{v}_g = \frac{v_{g1}^{-1} + v_{g2}^{-1}}{2}\,, \qquad \delta = \frac{1}{v_{g2}} - \frac{1}{v_{g1}}\,,$$
$$\beta_{2j} = \left.\frac{\mathrm{d}^2\beta_j}{\mathrm{d}\omega^2}\right|_{\omega=\omega_j}\,, \qquad \gamma_j = \frac{n_2\omega_j}{cS_j}\,,$$

α_j are the loss coefficients at the pump and probe frequencies, v_{gj} are the group velocities of the pump and probe pulses, n_2 is the nonlinear refractive index of the fiber material, and S_j are the effective mode areas of the pump and probe fields.

Neglecting optical losses, we represent the stationary solutions to Eqn (24) in the form

$$\bar{A}_j = \sqrt{P_j}\,\exp(\mathrm{i}\phi_j)\,, \tag{25}$$

where P_j is the power of the jth field, and $\phi_j = \gamma_j(P_j + 2P_{3-j})$ is the nonlinear phase shift.

We now consider small perturbations of the stationary solutions (25):

$$A_j = \left(\sqrt{P_j} + a_j\right)\exp(\mathrm{i}\phi_j)\,, \tag{26}$$
$$a_j = U_j\exp\left[\mathrm{i}(Kz - \Omega\tau)\right] + \text{c.c.}, \tag{27}$$

where U_j are the complex amplitudes of perturbations, K is the perturbation wave number, and c.c. stands for a complex-conjugate.

Substituting formulas (25)–(27) in Eqn (24) and linearizing the resulting set of equations with respect to the

perturbation amplitudes a_j, we derive the following dispersion relation for the perturbation wave number K [153]:

$$\left[\left(K-\frac{\Omega\delta}{2}\right)^2-h_1\right]\left[\left(K+\frac{\Omega\delta}{2}\right)^2-h_2\right]=C^2\,, \qquad (28)$$

where

$$h_j=\frac{1}{4}\,\beta_{2j}^2\,\Omega^2\left(\Omega^2+\frac{4\gamma_j P_j}{\beta_{2j}}\right), \qquad C=2\Omega^2\sqrt{\beta_{21}\beta_{22}\gamma_1\gamma_2 P_1 P_2}\,.$$

Stationary solutions (25) become unstable with respect to perturbations having wave numbers K with nonzero imaginary parts. Instabilities in the pump and probe fields are amplified under these conditions through parametric FWM with XPM-induced phase matching. The gain of such instabilities is given by the expression

$$G(\Omega)=2\,\mathrm{Im}\,(K)\,. \qquad (29)$$

We now use relationships (28) and (29) to analyze XPM-induced instabilities in PCFs employed in the experiments described below in this section. The fibers were fabricated from fused silica using a standard PCF technology [60] and had a cross-section structure shown in the inset to Fig. 5 with a core diameter of 4.3 μm. The group-delay parameter δ and the group-velocity dispersion $D=-2\pi c\lambda^{-2}\,\mathrm{d}^2\beta/\mathrm{d}\omega^2$ were calculated for the guided modes in such fibers by numerically solving the wave equation for the electric field. The numerical procedure [154] involved the expansion of the electric field in a set of orthogonal polynomials. The two-dimensional profile of the refractive index in the PCF cross section was represented as the sum over products of Hermite – Gauss polynomials and trigonometric functions.

Figures 6a and 6b display the group velocities and the GVD calculated as functions of radiation wavelength for the waveguide modes (mode profiles are shown in the insets to Fig. 6a) of the PCF considered. For the fundamental mode, as can be seen from Fig. 6b, the central wavelength of Cr:forsterite-laser radiation ($\lambda_1=2\pi c/\omega_1=1240$ nm) used in our experiments as a pump field fell within the range of anomalous dispersion. The second-harmonic output of this laser ($\lambda_2=2\pi c/\omega_2=620$ nm), which was used as a probe field in our measurements, lay in the region of normal dispersion. The group-delay parameter for the pump and probe pulses in the fiber considered was $\delta=20$ ps m^{-1}.

In Fig. 6c, we present the results of calculations performed with the use of formulas (28) and (29) for the gain of XPM-induced instability of the probe field with a central wavelength of 620 nm. These results [152] indicate a high efficiency of parametric frequency conversion of ultrashort laser pulses through XPM-induced instability. The central wavelength of the parametric signal generated as a result of this process is controlled by the group-delay parameter and the ratio of pump power P_1 to the power P_2 of the probe pulse. As the ratio P_1/P_2 changes from 1 to 6, the wavelength corresponding to the maximum gain G of parametric sideband generation with a fixed value of the group-delay parameter $\delta=20$ ps m^{-1}, as can be seen from Fig. 6c, is smoothly tuned within the range of wavelengths from 703 to 714 nm.

The laser system used in experiments [155] consisted of a Cr^{4+}:forsterite master oscillator, a stretcher, an optical isolator, a regenerative amplifier, a grating compressor, and a nonlinear crystal for frequency doubling. The master oscillator pumped with a fiber ytterbium laser generated 50 – 70-fs pulses of radiation with a central wavelength of 1250 nm and an average power of 180 mW at a repetition rate of 120 MHz. These light pulses were then transmitted through

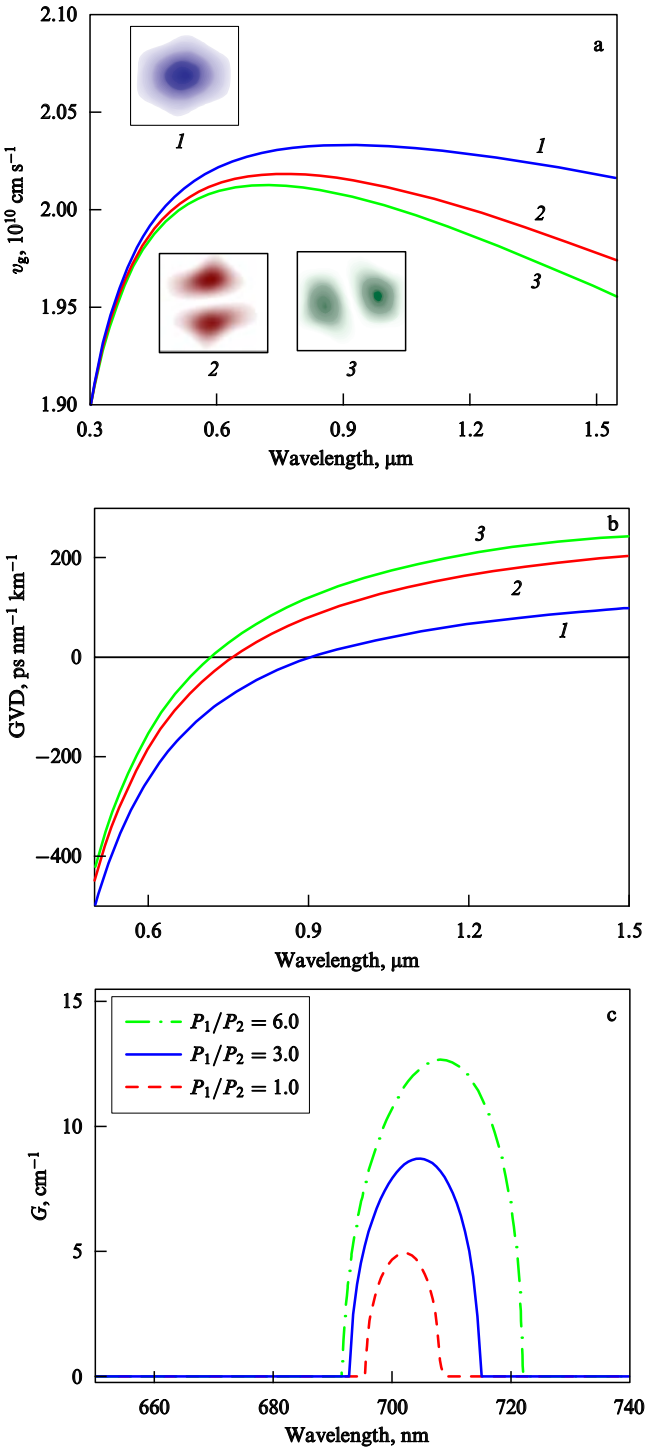

Figure 6. Group velocity (a) and group-velocity dispersion (b) as functions of radiation wavelength for three waveguide modes (curves *1 – 3*) in a PCF with a cross-section structure shown in the inset to Fig. 5. Field intensity profiles in waveguide modes *1 – 3* are shown in insets to Fig. 6a. (c) The gain of XPM-induced modulation instability, calculated as a function of radiation wavelength with the use of formulas (28) and (29) for different ratios of pump power P_1 to probe power P_2 in a PCF with a cross-section structure shown in the inset to Fig. 5. The central wavelength of the pump field is $\lambda_1=2\pi c/\omega_1=1240$ nm. The central wavelength of the probe field is $\lambda_2=2\pi c/\omega_2=620$ nm. The group-delay parameter is $\delta=20$ ps m^{-1}.

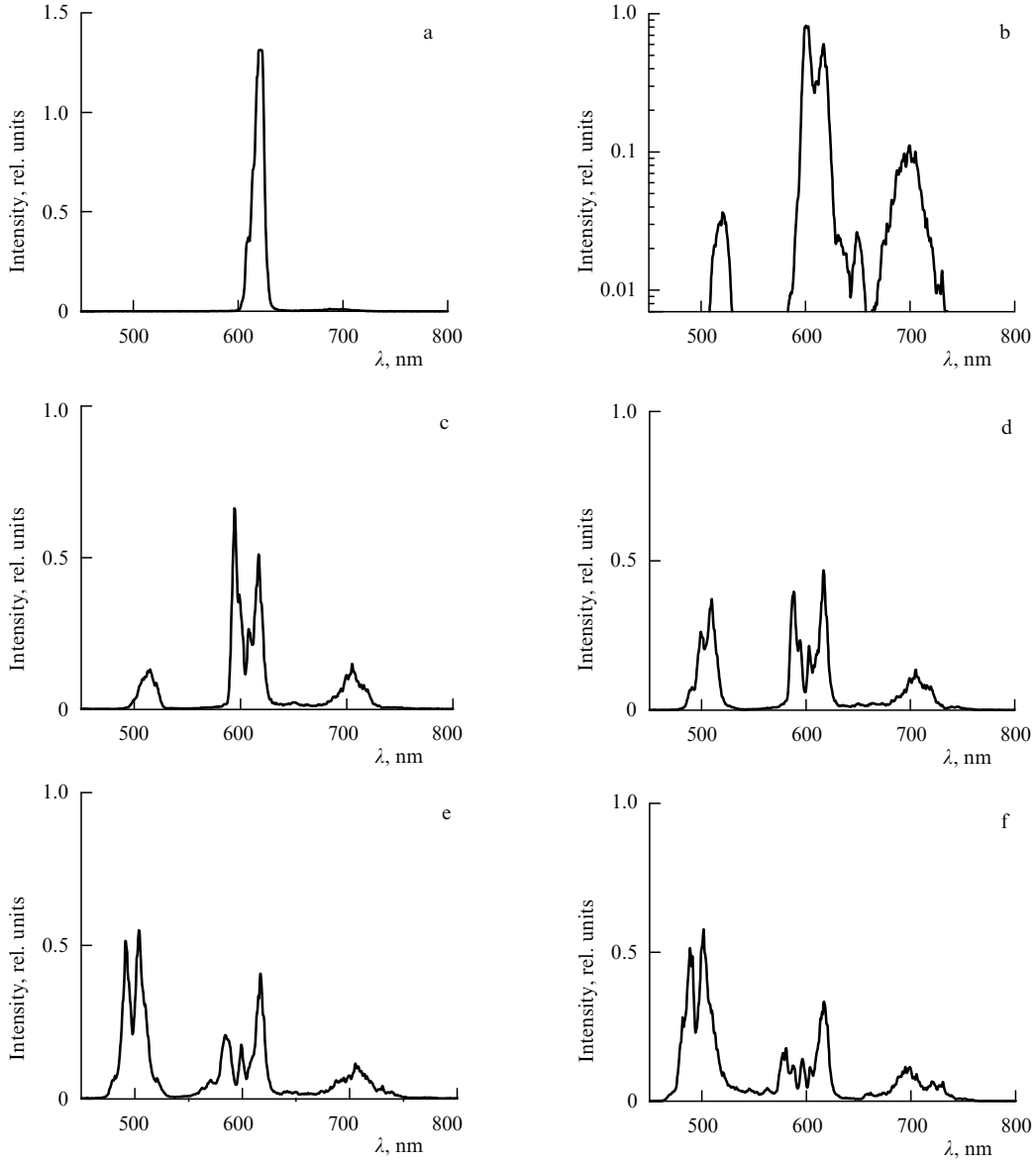

Figure 7. Spectra of a probe laser field transmitted through a 5-cm PCF. The peak power of the pump pulses is (a) 3 kW, (b) 7 kW, (c) 30 kW, (d) 42 kW, (e) 70 kW, and (f) 100 kW. The peak power of the probe pulse amounts to 8 kW.

a stretcher and an isolator, to be amplified in an Nd:YLF-laser-pumped regenerative amplifier and recompressed to the 50 – 150-fs pulse duration with a maximum laser pulse energy of about 100 μJ. An LBO crystal was utilized to generate the second harmonic of an amplified Cr:forsterite-laser radiation.

Experiments were performed with pump and probe pulses with an initial pulse width of about 100 fs. The energy of the probe pulse was fixed at a level of 2 nJ. The energy of the pump pulse was varied from 1 to 50 nJ. The fiber length was taken equal to 5 cm. For low pump energies, the probe pulse exhibited only a weak broadening at the output of the PCF (Fig. 7a) due to self-phase modulation.

Pump pulses of higher energies induced noticeable changes in the spectrum of the probe pulses at the output of the fiber (Figs 7b – 7f). Both the general tendencies of spectral transformation of the probe pulse and the specific frequencies of the sidebands observed in the spectrum of the probe field at the output of the PCF agree well with the results of our theoretical predictions. In particular, with an energy of the pump pulse equal to 14 nJ, the low-frequency component observed in the spectrum of the probe pulse at the output of the fiber is centered around 700 nm (Figs 7b – 7f). According to our calculations, this spectral region corresponds to the maximum gain G. As the pump-field power is increased, the central frequencies and the amplitudes of the sidebands in the spectrum of the probe field are smoothly tuned (Figs 7b – 7f). In particular, as the ratio P_1/P_2 increases from 3.5 to 7.0, the maximum of the low-frequency sideband in the spectrum of the probe pulse, as can be seen from Fig. 7, is shifted from 702 to 712 nm, which agrees well with the calculated results (Fig. 6c). Thus, both the main tendencies and the most significant quantitative parameters of sideband generation in the spectrum of a probe femtosecond pulse in the presence of a copropagating pump pulse in our PCF can be adequately understood in terms of the standard model of XPM-induced modulation instability.

Results of experimental and theoretical studies, presented in this section, suggest potentials of using XPM-induced modulation instability for efficient parametric frequency conversion of low-power femtosecond laser pulses. The

amplitudes and the frequency shifts of the sidebands generated in the spectrum of the probe field at the output of the fiber as a result of parametric four-wave mixing are controlled by varying the intensity of the pump field.

6.2.2 Soliton self-frequency shift. Nonstationary spectral transformations of ultrashort laser pulses in media with noninstantaneous optical nonlinearity are often accompanied by a continuous downshift of the central frequency [133, 134]. For Raman-active media, this effect is illustratively interpreted in the frequency domain [32] as the amplification of the low-frequency part of the spectrum of an ultrashort pulse by its high-frequency wing through stimulated Raman scattering. As a result, the carrier frequency of an ultrashort pulse propagating through a Raman-active medium in a solitonic regime undergoes a permanent red shift. This phenomenon, called soliton self-frequency shift (SSFS), allows the creation of fiber-optic frequency shifters for ultrashort laser pulses. Due to the strong confinement of the light field in a small-area fiber core, PCFs can radically increase the SSFS rate [156]. Special dispersion profiles of waveguide modes can be designed by optimizing the PCF structure to improve the coupling of low-energy ultrashort laser pulses to frequency-shifting solitons [157]. As a result, the soliton self-frequency shift in PCFs enables a smooth wavelength tuning of low-energy few-cycle field waveforms [158], suggesting a reliable and convenient method for the synchronization of pump and seed pulses in optical parametric chirped-pulse amplification [159].

The initial pulse width is one of the key parameters controlling the SSFS regime. According to the SSFS analysis based on the nonlinear Schrödinger equation with an assumption of a linear frequency dependence of the Raman gain $R(\nu)$ [160], the shift rate of the central frequency ν_0 of the soliton propagating along the z-axis is highly sensitive to the soliton pulse width τ_0: $\mathrm{d}\nu_0/\mathrm{d}z \propto \tau_0^{-4}$. Deviation of $R(\nu)$ from a linear function and high-order dispersion effects can violate the scaling law $\mathrm{d}\nu_0/\mathrm{d}z \propto \tau_0^{-4}$. It would be natural to expect that deviations from this scaling law should become quite dramatic for pulses with an initial duration τ_0 less than the period τ_R of the Raman mode ($\tau_\mathrm{R} \approx 80$ fs for fused silica [32]). Experimental studies of the SSFS in the regime where $\tau_0 \ll \tau_\mathrm{R}$ have demonstrated [157, 158] that spectral shifts exceeding 180 THz can be achieved for pulses with an initial duration $\tau_0 \approx 6$ fs and an appropriate profile of the spectral phase.

Serebryannikov et al. [161] have examined specific features of soliton self-frequency shift of subnanojoule ultrashort laser pulses in PCFs in the regime where $\tau_0 < \tau_\mathrm{R}$. The results of these experiments show that the SSFS rate can be substantially increased by reducing the input pulse width. Solitonic frequency shifts exceeding 100 THz have been achieved for subnanojoule Ti:sapphire-laser pulses with an initial pulse width of about 30 fs, transmitted through a PCF with a core diameter of about 1.6 μm and a length of about 7 cm.

Analysis of the spectral and temporal soliton dynamics in PCFs is based on the numerical solution to the generalized nonlinear Schrödinger equation [52]

$$\frac{\partial A}{\partial z} = \mathrm{i}\sum_{k=2}^{6} \frac{\mathrm{i}^k}{k!}\,\beta^{(k)}\,\frac{\partial^k A}{\partial \tau^k} + \mathrm{i}\gamma\left(1 + \frac{\mathrm{i}}{\omega_0}\,\frac{\partial}{\partial \tau}\right) \times A(z,\tau)\int_{-\infty}^{\infty} R(\eta)\left|A(z,\tau-\eta)\right|^2 \mathrm{d}\eta\,, \qquad (30)$$

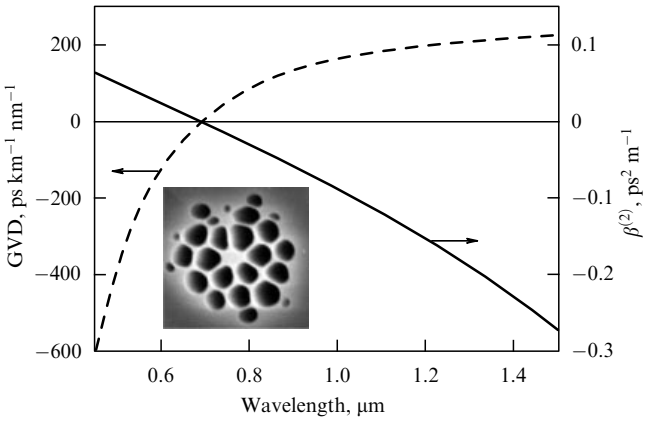

Figure 8. Group-velocity dispersion (dashed line) and the coefficient $\beta^{(2)}$ (solid line) as the functions of radiation wavelength for the fundamental mode of a PCF with the cross-section structure shown in the inset.

where A is the pulse envelope, $\beta^{(k)} = \partial^k\beta/\partial\omega^k$ are the coefficients in the Taylor-series expansion for the propagation constant β of the relevant guided mode, ω_0 is the carrier frequency, τ is the time in the retarded frame of reference, $\gamma = n_2\omega_0/(cS_\mathrm{eff})$ is the nonlinearity coefficient, n_2 is the refractive index controlling the Kerr additive to the refractive index, S_eff is the effective area of the waveguide mode, and $R(t)$ is the retarded nonlinear response. For fused silica, we set $n_2 \approx 3.2 \times 10^{-16}$ cm^2 W^{-1} and employ the following model of the Raman response [52, 162]:

$$R(t) = (1 - f_\mathrm{R})\,\delta(t) + f_\mathrm{R}\Theta(t)\,\frac{\tau_1^2 + \tau_2^2}{\tau_1\tau_2^2}\exp\left(-\frac{t}{\tau_2}\right)\sin\left(\frac{t}{\tau_1}\right), \qquad (31)$$

where $f_\mathrm{R} = 0.18$ is the fraction of the Raman effect in the total nonlinear response, $\delta(t)$ is the delta function, $\Theta(t)$ is the Heaviside step function, while $\tau_1 = 12.5$ fs and $\tau_2 = 32$ fs are typical times for the Raman response in fused silica.

Parameters $\beta^{(k)}$ were calculated by numerically solving the Maxwell equations for the transverse components of the electric and magnetic fields using the method of Hermite–Gauss polynomial expansions [161]. Simulations were performed for a fused-silica PCF with a core diameter of 1.6 μm and the structure of cross section shown in the inset to Fig. 8. The frequency dependences of propagation constants β calculated with the use of this procedure were represented as polynomials

$$\beta(\omega) = \beta(\omega_0) + \sum_{k=1}^{6}\frac{\beta^{(k)}}{k!}(\omega - \omega_0)^k\,.$$

The confidence level for the errors of this polynomial fit in the range of wavelengths from 580 to 1220 nm was taken equal to 0.1%. For the central frequency ω_0 corresponding to a wavelength of 800 nm, the required accuracy was achieved with the following set of expansion coefficients: $\beta^{(2)} \approx -0.0293$ ps^2 m^{-1}, $\beta^{(3)} \approx 9.316 \times 10^{-5}$ ps^3 m^{-1}, $\beta^{(4)} \approx -9.666 \times 10^{-8}$ ps^4 m^{-1}, $\beta^{(5)} \approx 1.63 \times 10^{-10}$ ps^5 m^{-1}, and $\beta^{(6)} \approx -3.07 \times 10^{-13}$ ps^6 m^{-1}. The fact that $\beta^{(2)}$ is negative implies that the 800-nm wavelength falls within the range of anomalous dispersion. Femtosecond pulses with such a central frequency can therefore be coupled to solitons in the PCF considered. The group-velocity dispersion and the

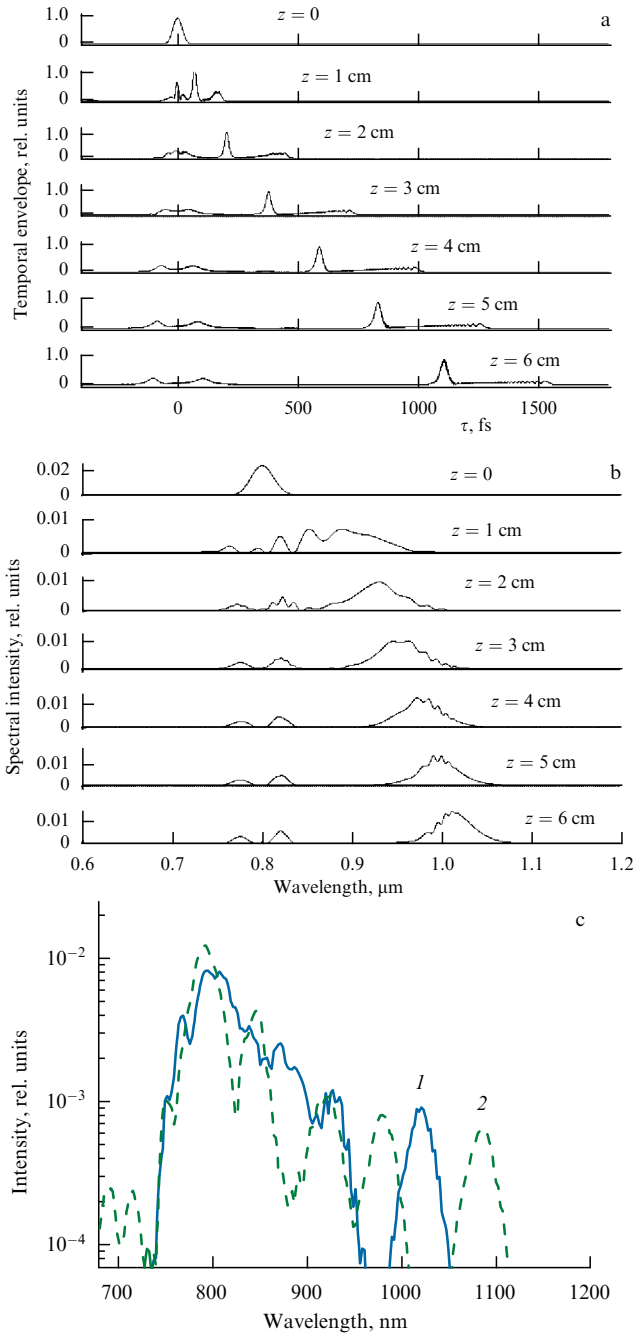

Figure 9. Evolution of the temporal envelope (a) and the spectral intensity (b) of a laser pulse with an initial pulse width of 30 fs and an energy of 0.3 nJ, propagating along the z-axis in a PCF. (c) The spectrum of a Ti:sapphire-laser pulse transmitted through a 7-cm PCF. The initial pulse width is 30 fs. The input pulse energy is (*1*) 340 pJ, and (*2*) 540 pJ.

coefficient $\beta^{(2)}$ as functions of radiation wavelength for the fundamental mode of the PCF are shown in Fig. 8. The GVD vanishes, as can be seen from these plots, at the wavelength $\lambda_z \approx 690$ nm.

Figures 9a and 9b display the spectral and temporal evolution of a pulse with an initial width of 30 fs, propagating through a PCF with the above-specified dispersion coefficients $\beta^{(k)}$. Characteristic isolated features appearing in the spectrum and temporal envelope of the field indicate the formation of solitons. A finite response time of nonlinearity leads to the red shifting of solitonic structure frequencies — a typical SSFS scenario. In the regime of anomalous dispersion, low-frequency components of the radiation field are slower than high-frequency components. As a result, Raman solitons become isolated from the nonsolitonic part of the field in both time (Fig. 9a) and wavelength (Fig. 9b) domains.

Numerical simulations indicate that shorter pulses noticeably enhance SSFS in PCFs. This result agrees well with predictions of earlier studies [160] into the SSFS based on the analysis of the nonlinear Schrödinger equation. To provide qualitative physical insights into this tendency, we consider here the properties of the function

$$\Psi(z,\tau) = \int R(\eta)\left|A(z,\tau-\eta)\right|^2 \mathrm{d}\eta$$

which controls the red shifting in Eqn (30) governing the evolution of an ultrashort pulse. The function $\Psi(z,\tau)$ is given by a convolution of the temporal envelope of the field intensity and the retarded (Raman) response $R(t)$ of the nonlinear material. The Raman response $R(t)$ of fused silica is adequately approximated [see Eqn (31)] with a rapidly damped oscillating function with the period $\tau_R = 2\pi\tau_1 \approx 80$ fs. For light pulse widths $\tau_0 \gg \tau_R$, the function $\Psi(z,\tau)$ closely follows the temporal envelope of the radiation field intensity. The influence of the finite response time of nonlinearity is weak in this regime, and the red shifting of the Raman soliton is characterized by lower rates $\mathrm{d}v_0/\mathrm{d}z$.

For short laser pulses, $\tau_0 < \tau_R$, the function $\Psi(z,\tau)$ can noticeably differ from the temporal profile of the field intensity. Deviation of $\Psi(z,\tau)$ from the temporal profile of the light intensity increases for shorter input pulses, thus leading to higher SSFS rates $\mathrm{d}v_0/\mathrm{d}z$. Numerical analysis of soliton dynamics in a PCF shows that, as the initial pulse width is reduced from 50 to 30 fs, the soliton frequency shift in the PCF with a length of 7 cm increases by a factor of 1.5–2 for the above-specified dispersion profile.

During experimental studies [161], an argon-laser-pumped self-starting Ti:sapphire laser with SESAM mirrors was employed. Laser radiation was coupled into a PCF (see the inset to Fig. 8) with the use of standard micro-objectives. The spectra of radiation coming out of the fiber were measured by an Ando spectrum analyzer. The mode structure of output radiation was controlled with the aid of a CCD camera.

The energy of the input laser pulse was chosen in such a way as to provide formation of the fundamental soliton. The energy of 30-fs laser pulses coupled into the fiber was estimated as 0.3 nJ. In agreement with the results of numerical simulations (Figs 9a, b), the initial stage of pulse propagation involved rather complicated spectral and temporal dynamics of laser pulses. Nonlinear-optical spectral transformation of laser pulses under these conditions is dominated by self-phase modulation, stimulated Raman scattering, and parametric four-wave mixing.

Within a propagation length of a few centimeters, we observed formation of red-shifted isolated frequency components (Fig. 9c). Pulses with an initial duration of 30 fs, transmitted through a 7-cm PCF section, gave rise to a red-shifted component with a central wavelength of about 1020 nm (line *1* in Fig. 9c). The frequency shift of this component with respect to the central frequency of the input field exceeded 100 THz. Higher input radiation energies in these experiments did not necessarily result in a noticeable

increase in the maximum soliton frequency shift, which can be attributed to the excitation of high-order guided modes and the formation of high-order solitons (line *2* in Fig. 9c).

The experimental studies and numerical simulations presented above in this section reveal interesting features of the soliton self-frequency shift of laser pulses with initial pulse widths less than the period of the Raman mode of the nonlinear material. In particular, the rate of soliton self-frequency shift can be substantially increased by reducing the initial pulse width. A typical frequency shift of subnanojoule Ti:sapphire-laser pulses with an initial duration of about 30 fs, transmitted through a PCF with a core diameter of about 1.6 μm and a length of about 7 cm, exceeds 100 THz.

Because of the sensitivity of the SSFS to the parameters of the input pulse, small fluctuations in the input laser power can give rise to undesirable variations in the central wavelength of the frequency-shifted solitonic fiber output with a related timing jitter of the time-delayed soliton. This factor limits the accuracy of the time synchronization of a frequency-shifted soliton with an ultrashort seed pulse in optical parametric chirped-pulse amplification based on SSFS [159]. However, as shown in Refs [163, 164], the initial stage of a fast SSFS is sometimes followed by a regime where the soliton frequency shifting slows down. The frequency dependence of the GVD and the diffraction-induced increase in the effective mode area for longer wavelengths tend to arrest the SSFS around an asymptotic limit controlled by the dispersion profile and the frequency dependence of the effective mode area. The numerical analysis of the generalized nonlinear Schrödinger equation (30) with a specific frequency dependence of the effective mode area demonstrates that the frequency shift of a soliton [165, 166], as well as the frequency shift of an ultrashort pulse of a more general type [167], becomes arrested as the pulse travels along an optical fiber. Numerical simulations performed in Refs [165, 166] show that, with an appropriate PCF design, the suppression of the SSFS due to the frequency dependence of the effective mode area can substantially reduce unwanted variations in the central wavelength and the timing jitter of the frequency-shifted solitonic PCF output. In this regime, the accuracy of time synchronization between the pump and seed pulses in optical parametric chirped-pulse amplification based on the SSFS in a PCF [159] can be radically improved.

6.2.3 Soliton instability and dispersive-wave radiation. The remarkable stability of soliton solutions to nonlinear Schrödinger equation (22) is due to the fact that the spectrum of solitonic wave numbers lies away from the dispersion region of linear dispersive waves. A wave-number mismatch between a soliton and a manifold of dispersive waves prevents energy transfer from a soliton to dispersive waves. Solitons are, however, unstable with respect to perturbations whose wave numbers belong to the solitonic spectrum. Such perturbations can be induced, for example, by high-order dispersion [135, 136]. Resonant energy exchange between a soliton and linear dispersive waves induced by high-order dispersion is one of the main mechanisms responsible for the generation of the visible portion of supercontinuum radiation in PCFs [168].

To illustrate the main features of solitonic instabilities giving rise to the generation of blue-shifted spectral components, we represent the propagation constant β_s of a soliton at the frequency ω as a power series

$$\beta_s(\omega) = \beta(\omega_s) + \frac{1}{u}(\omega - \omega_s) + \frac{\gamma P}{2}\,, \tag{32}$$

where ω_s is the central frequency of the soliton spectrum.

The propagation constant of a dispersive guided mode at the frequency ω is written down as

$$\beta(\omega) = \beta(\omega_s) + \frac{1}{u}(\omega - \omega_s) + \frac{\beta_2}{2}(\omega - \omega_s)^2 + \frac{\beta_3}{6}(\omega - \omega_s)^3\,, \tag{33}$$

where $\beta_3 = \partial^3\beta/\partial\omega^3|_{\omega=\omega_s}$ is the third-order dispersion.

A soliton can resonantly transfer its energy to a dispersive wave at the frequency $\Omega = \omega - \omega_s$ that meets the condition

$$\Delta\beta(\Omega) = \beta(\Omega) - \beta_s(\Omega) = \beta_2\,\frac{\Omega^2}{2} + \beta_3\,\frac{\Omega^3}{6} - \frac{\gamma P}{2} = 0\,. \tag{34}$$

In the low-power regime, when the term $\gamma P/2$ is much less than the other two terms in Eqn (34), the resonant energy exchange between a soliton and a dispersive wave occurs at the frequency

$$\Omega_0 \approx -\frac{3\beta_2}{\beta_3}\,. \tag{35}$$

In the region where solitons exist, we have $\beta_2 < 0$ (anomalous dispersion). Near the zero-GVD wavelength, the inequality $\beta_3 > 0$ has to hold true in the region of anomalous dispersion. The frequency offset Ω is then positive, with the resonant energy exchange between a soliton and dispersive waves giving rise to the generation of blue-shifted (relative to the central wavelength of the soliton) spectral components.

With $P \neq 0$, the cubic equation (34) can be solvable exactly for Ω using the Cardano formula [169]. For small P, an approximate solution to this equation can be found by an iterative procedure:

$$\Omega \approx \Omega_0\left(1 - \frac{\gamma P}{\beta_2\Omega_0^2}\right). \tag{36}$$

If the fourth-order dispersion plays a more important role than the third-order dispersion, so that the propagation constant of the dispersive mode can be written as

$$\beta(\omega) = \beta(\omega_s) + \frac{1}{u}(\omega - \omega_s) + \frac{\beta_2}{2}(\omega - \omega_s)^2 + \frac{\beta_4}{24}(\omega - \omega_s)^4\,, \tag{37}$$

where $\beta_4 = \partial^4\beta/\partial\omega^4|_{\omega=\omega_s}$, a low-$P$ soliton can resonantly transfer its energy to a dispersive wave at the frequency

$$\bar{\Omega}_0 \approx \pm\left(-\frac{12\beta_2}{\beta_4}\right)^{1/2}. \tag{38}$$

An important property of energy transfer from a soliton to a dispersive wave is related to the nature of phase matching between the soliton and the dispersive wave it radiates. Since the phase velocity of the soliton traveling along the fiber axis is higher than the phase velocity of the dispersive wave being emitted, the soliton resonance radiation is observed at a certain angle to the fiber axis [136]. In this respect,

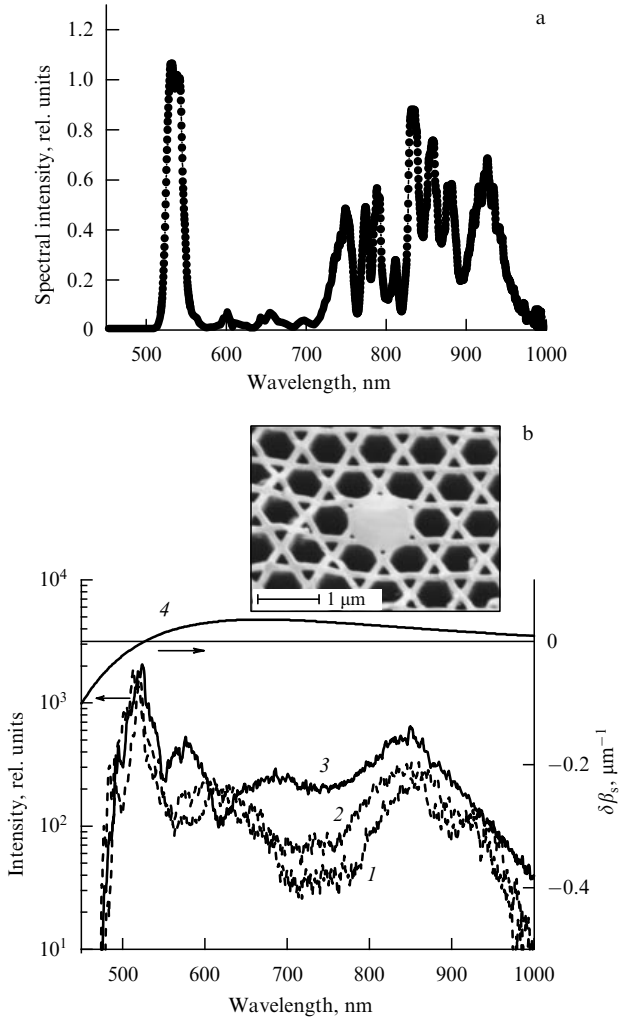

Figure 10. (a) The spectrum of unamplified Ti:sapphire laser pulses with an initial pulse width of 50 fs, transmitted through off-center waveguide microchannels in a 10-cm PCF with the cross-section structure shown in the inset to Fig. 5. (b) Spectra of Cr:forsterite laser pulses transmitted through a 12-cm piece of a multicomponent-glass photonic-crystal fiber with a cross-section structure shown in the inset and a core diameter of 2 μm. The input laser pulses have a pulse width of 200 fs and an energy of (*1*) 20 nJ, (*2*) 30 nJ, and (*3*) 40 nJ. Curve *4* shows the propagation-constant mismatch $\delta\beta_s$ between the soliton centered at 1.25 μm and dispersive waves guided by the fundamental mode of the PCF as a function of the wavelength of the dispersive wave.

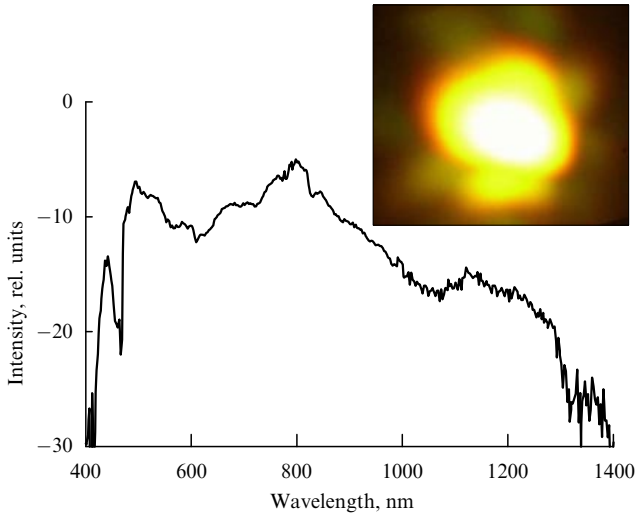

Figure 11. The spectrum of supercontinuum radiation produced by unamplified 820-nm Ti:sapphire-laser pulses with an initial duration of 35 fs and an input power of 320 mW in a fused silica PCF with a length of 30 cm and the cross-section structure shown in the inset to Fig. 8.

dispersive-wave emission by solitons is similar to electromagnetic radiation emitted by a charged particle moving in a medium with a speed exceeding the phase velocity of the wave being radiated. By analogy with electromagnetic radiation emitted by fast charged particles, dispersive-wave radiation by solitons is often referred to as Cherenkov radiation [136].

Cherenkov radiation of solitons manifests itself as intense spectral lines blue-shifted with respect to the central wavelength of input radiation. In the regime of supercontinuum generation these spectral lines are observed in the short-wavelength part of the white-light spectrum. Such blue-shifted spectral components can be generated when at least some part of the input spectrum falls within the region of anomalous dispersion of the waveguide mode or gets transferred into this region through nonlinear-optical interactions in the fiber (Fig. 4b). Figure 10 presents typical radiation spectra at the output of PCFs performing a frequency conversion of femtosecond Ti:sapphire (Fig. 10a) and Cr:forsterite (Fig. 10b) laser pulses through Cherenkov soliton emission. Curve *4* in Fig. 10b displays the mismatch of the propagation constants of the soliton and dispersive wave, $\delta\beta_s = \beta_s(\lambda_0) - \beta(\lambda)$, calculated for the given PCF structure as a function of the wavelength λ for a soliton with the central wavelength $\lambda_0 = 1.25$ μm. As can be seen from Fig. 10b, the spectral peak in the visible region of the spectrum is observed at the wavelength corresponding to the phase-matching condition $\delta\beta_s = 0$.

For higher input laser energies or longer fibers, solitons of high orders can be produced in the fiber, increasing the spectral interval of a resonant energy exchange between solitons and dispersive waves. Long-wavelength spectral components can simultaneously undergo broadening and shifting due to SPM, FWM, modulation instabilities, SRS, and SSFS. These processes give rise to radiation with a broadband spectrum at the output of the fiber, which is observed as bright white-light emission (see Fig. 4a and the inset to Fig. 11). The bandwidth of this radiation may reach several octaves, with its spectrum spanning over the entire visible and a considerable part of the near-infrared regions. In Section 7, we will discuss applications of PCF sources of white light and frequency converters in optical metrology, as well as in nonlinear spectroscopy and microscopy.

6.3 Optical fibers of highly nonlinear materials

The high optical nonlinearity of PCFs is related to their structure confining electromagnetic radiation in a small-diameter fiber core due to a high refractive-index step between the core and the cladding of the fiber. The most common fused silica PCFs are typically classified as highly nonlinear when their nonlinear coefficient γ is on the order of 100 W^{-1} km^{-1}. A radical increase in γ above this value is prevented by the low nonlinearity of silica, whose nonlinear refractive index is $n_2 \approx (2-3) \times 10^{-16}$ cm^2 W^{-1}. However, higher nonlinear coefficients can be achieved with other materials that possess much higher optical nonlinearities and that are compatible with fiber-optic technologies (see

Ref. [170] for a review of such materials). Analysis of the capabilities and waveguide properties of PCFs made of highly nonlinear materials is of considerable interest for nonlinear fiber optics, including the development of fiber-optic supercontinuum radiation sources.

A promising class of waveguides for nonlinear optics includes PCFs fabricated with the use of lead silicate glasses. Petropoulos et al. [171] have examined the properties of SF_{57} PCFs. The nonlinear refractive index of this type of glass at a wavelength of 1060 nm can be as high as $n_2 \approx 4.1 \times 10^{-15}$ cm^2 W^{-1}, i.e., more than an order of magnitude higher than the nonlinear refractive index of fused silica. The nonlinear coefficient of PCFs fabricated of such glasses can reach 640 W^{-1} km^{-1}. The zero-GVD wavelength of bulk SF_{57} glass is about 1970 nm, making it possible to design PCFs with dispersion profiles suitable for efficient frequency conversion of erbium-laser pulses with a central wavelength around 1550 nm. The authors of Ref. [171] reported efficient generation of Raman solitons in a short, 37-cm segment of an SF_{57} PCF pumped by erbium-laser pulses with an input energy of about 50 pJ, a pulse width of about 1.5 ps, and a repetition rate of 1.5 GHz.

Kanth Kumar et al. [172] have reported manufacture of soft-glass SF_6 PCFs. The nonlinear refractive index for such glasses is $n_2 \approx 2.2 \times 10^{-15}$ cm^2 W^{-1}. At a wavelength of 1550 nm, the GVD in the bulk of SF_6 glass is normal. For PCFs with core diameters of 2.6 or 4.0 μm, the GVD passes through zero around the wavelengths of 1.3 and 1.4 μm, respectively. Fibers of this type can provide a high efficiency of supercontinuum generation [173] with a pump provided by an all-fiber erbium oscillator–amplifier system delivering light pulses with a central wavelength of 1560 nm, a pulse width of about 60 fs, an energy of about 200 pJ, and a pulse repetition rate of about 60 MHz. A high efficiency of spectral transformation of femtosecond pulses produced by erbium fiber lasers is provided by germanium-doped dispersion-shifted silica fibers [174]. A typical nonlinearity coefficient for such fibers at the wavelength of 1550 nm equals $\gamma \approx 10$ W^{-1} km^{-1}. Nicholson et al. [175] have demonstrated efficient supercontinuum generation in such fibers using pump pulses generated by an erbium fiber oscillator–amplifier laser with a central wavelength of 1550 nm, a pulse width of 180 fs, and an average power of about 50 mW. Tellurite-glass PCFs can efficiently SRS-transform 1064-nm subnanosecond laser pulses with an energy of about 1 μJ [176].

Chalcogenide glass is of special interest for nonlinear waveguide and fiber optics [177]. The nonlinear refractive index for the materials of this class can be as high as 10^{-13} cm^2 W^{-1}. Certain types of chalcogenide glass are transparent in the infrared spectral region up to 5 μm and possess high Raman gains. Due to these properties, chalcogenide glass can be employed for the creation of waveguide and fiber-optic switches and sensors, as well as fiber-optic Raman lasers and amplifiers in the near-, mid-, and far-infrared regions [178]. Fabrication of chalcogenide-glass PCFs and investigation of their properties were reported on by Monro et al. [179].

The inset to Fig. 10b and Fig. 12a display cross-section images of multicomponent-glass PCFs designed for the spectral transformation of femtosecond Cr:forsterite-laser pulses [180]. In spite of rather high nonlinearities provided by silica PCFs with core diameters less than 2–2.5 μm, such fibers cannot always provide an efficient transformation of

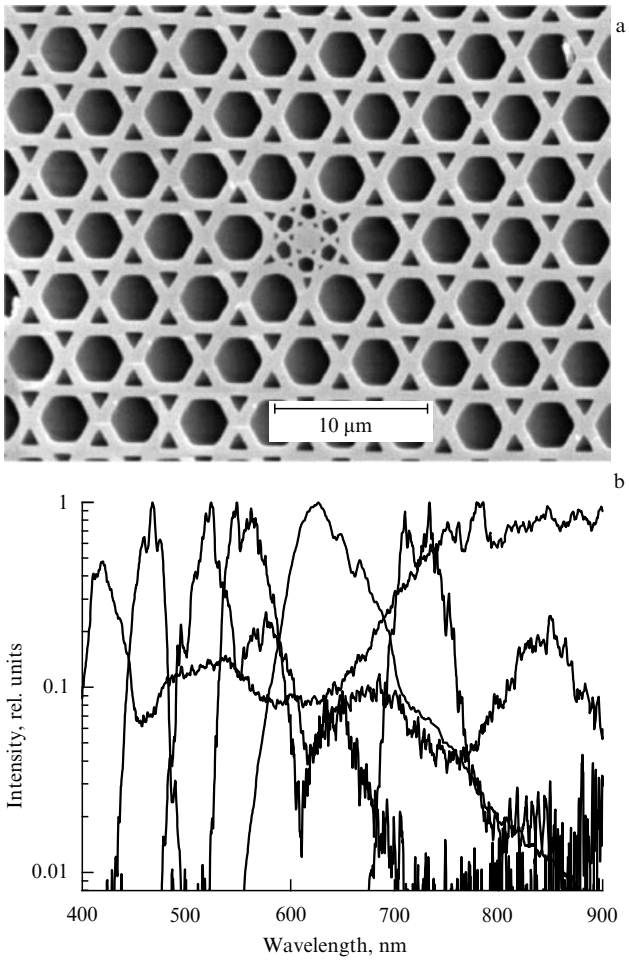

Figure 12. (a) Cross-section image of a multicomponent-glass PCF. (b) Intensity spectra of femtosecond Cr:forsterite-laser pulses transmitted through the PCF of this type. The central wavelength of the blue-shifted PCF output is tuned by changing the offset $\delta\lambda = |\lambda_0 - \lambda_z|$, where λ_0 is the central wavelength of the input field, and λ_z are the zero-GVD wavelengths of the PCF.

Cr:forsterite-laser radiation into broadband emission with a smooth spectrum at the fiber output. In the above-specified range of core diameters, the central wavelength λ_0 of Cr:forsterite-laser radiation lies too far from the zero-GVD wavelength λ_z, which gives rise to a noticeable gap between the long-wavelength, solitonic part of the output spectrum and its short-wavelength part dominated by the Cherenkov emission of solitons and FWM processes (see Sections 5 and 6.2). Multicomponent glass used to fabricate the PCF shown in the inset to Fig. 10b has a nonlinear refractive index n_2 close to that of fused silica. However, dispersion properties of the multicomponent glass allow the wavelength detuning $\delta\lambda = |\lambda_0 - \lambda_z|$ to be reduced without increasing the fiber core diameter, i.e., without the loss in the nonlinearity of the PCF structure (see the inset to Fig. 13). For multicomponent-glass PCFs with core diameters equal to 2.0 and 2.4 μm, the GVD passes through zero (curves *1* and *2* in Fig. 13) at 910 and 980 nm, respectively. For silica PCFs with the same core diameters, zero GVD is achieved (curves *3* and *4* in Fig. 13) at 715 and 767 nm, respectively. Thus, multicomponent-glass PCFs with the above-specified parameters are better suited for a supercontinuum transformation of Cr:forsterite laser pulses.

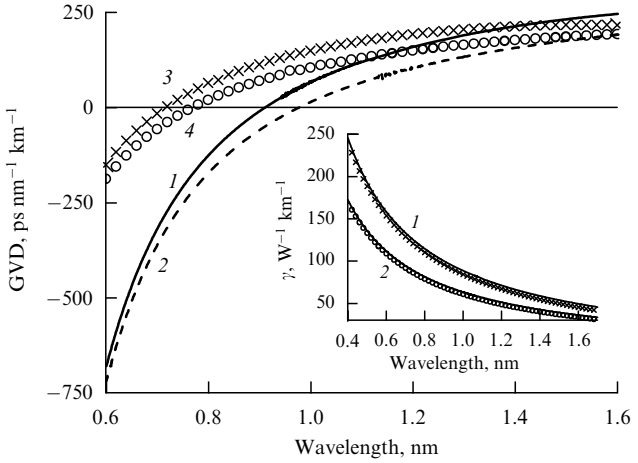

Figure 13. Group-velocity dispersion as a function of the wavelength for multicomponent-glass PCFs with the cross-section structure shown in the inset to Fig. 10b and a core diameter of (*1*) 2.0 μm, and (*2*) 2.4 μm. Curves *3* and *4* depict the GVD for the fundamental mode in a silica PCF with the same structure and a core diameter of 2.0 and 2.4 μm, respectively. The inset presents the nonlinear coefficient γ as a function of the wavelength for the same type of PCF with a core diameter of (*1*) 2.0 μm, and (*2*) 2.4 μm. The wavelength dependences of the nonlinear coefficient γ for a silica PCF with a core diameter of 2.0 μm (crosses) and 2.4 μm (circles) are plotted for comparison.

Figure 12b depicts the results of spectral measurements performed with several multicomponent-glass PCFs having the same type of cross-section structure (shown in Fig. 12a) but different magnification factors of the structure as a whole, varied at the stage of fabrication. Such a family of PCFs, as is seen from the experimental results presented, can wavelength-convert femtosecond Cr:forsterite-laser pulses to any output wavelength within the range from 400 to 900 nm. This method of frequency conversion of femtosecond Cr:forsterite-laser pulses opens up fresh opportunities for nonlinear spectroscopy (see Section 7.2), as well as for time-resolved studies of ultrafast processes in molecular systems by means of laser-induced fluorescence [180].

Another important class of materials allowing highly efficient frequency conversion of laser radiation and white-light generation includes materials with a high Raman gain [181, 182]. An increase in the fraction of the retarded nonlinearity in the intensity-dependent refractive index of a nonlinear medium [the factor f_R in the generalized nonlinear Schrödinger equation (30)] may qualitatively change the spectral transformation of ultrashort pulses in the regime of anomalous dispersion relative to the well-known scenario of spectral broadening, involving frequency-shifting solitons, observed in silica fibers. This effect is illustrated by the results of numerical simulations performed by Serebryannikov et al. [183] for tellurite fibers with a Raman gain being approximately 50 times higher than the Raman gain of silica fibers. The fraction of the Raman part of nonlinearity in the intensity-dependent refractive index for the considered type of glass ($f'_R \approx 0.76$) is much higher than the factor f_R for silica ($f_R \approx 0.18$). As a result, the continuously frequency-shifting solitonic peaks, typically observed in the temporal field intensity envelope for silica fibers (Fig. 14a), are transformed in the tellurite fibers under consideration into intensity-envelope peaks with a rapidly changing amplitude and pulse width, observed against a powerful background related to the nonsolitonic part of the radiation field

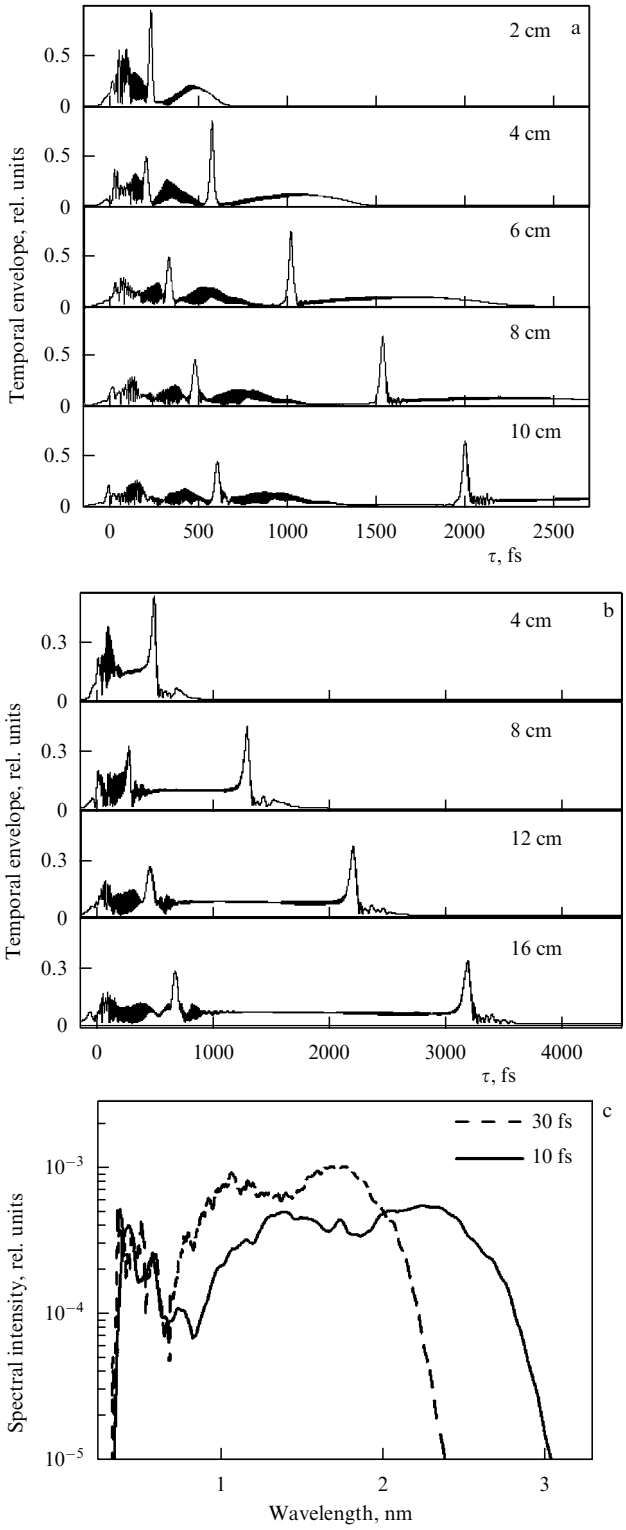

Figure 14. Time evolution of a laser pulse with an initial pulse width of 30 fs in a silica (a) and tellurite (b) PCFs. The input pulse energy is chosen in such a way as to provide the excitation of a fundamental soliton in the fiber. (c) Supercontinuum generation in a tellurite PCF with a length of 3 cm. The initial pulse width is 10 fs (solid line), and 30 fs (dashed line). The input pulse energy is 1.0 nJ.

(Fig. 14b). A high Raman gain can thus prevent the formation of stable solitonic features isolated in the time and frequency domains from the nonsolitonic part of the field. With an input peak power corresponding to a multi-

soliton regime, fibers made of high-Raman-gain materials can serve, as demonstrated in Fig. 14c, as efficient white-light sources in the visible and near-infrared spectral regions.

7. Applications of fiber-optic white-light sources

7.1 Supercontinuum generation and revolution in optical metrology

In this section we examine applications of PCFs in systems of optical metrology. PCFs have been at the heart of revolutionary changes of the past few years in optical metrology, leading to a radical simplification of metrology-oriented laser systems [78 – 80]. Within the past five to six years, technically and conceptually sophisticated multistage systems of optical metrology and high-precision spectroscopy have been replaced by compact table-top devices providing an unprecedentedly high accuracy of fundamental optical measurements [81], celebrated by the Nobel Prize in Physics 2005.

The key concept underlying the latest breakthroughs in optical metrology involves using frequency combs [184 – 186] generated by mode-locked femtosecond lasers for the measurement of frequency intervals (Fig. 15). Mode-locked femtosecond lasers deliver sequences of light pulses separated by a time interval T equal to the round-trip time of the laser cavity. In the frequency domain, such pulse trains are represented by equidistant frequency combs (see Fig. 15) with a total spectral width determined by the time width of the laser pulses in the train and a frequency interval $\Delta\omega$ between the adjacent spectral components equal to $\Delta\omega = 2\pi/T$. Such a frequency comb can be calibrated against an atomic frequency standard and employed as a ruler measuring spectral and, hence, temporal and spatial intervals. Thus, while optical spectroscopy conventionally deals with wavelength measurements, the new concept in optical metrology involves the measurement of frequency intervals by using frequency rulers, improving the precision of optical measurements by many orders of magnitude and allowing the creation of a new generation of frequency standards and optical clocks [81]. The significance of this concept for optical metrology and high-precision laser spectroscopy has been highlighted by the statement of the Nobel Committee for Physics concerning the Nobel Prize in Physics 2005, which specifically mentions the frequency-comb measurement technique [9].

The idea of using mode-locked laser sources of short pulses for high-precision optical measurements was proposed in the late 1970s [187, 188]. Hänsch's group was the first to experimentally demonstrate high-precision fine-structure measurements on atomic energy levels using frequency combs generated by picosecond mode-locked lasers. With the total width of the frequency comb being inversely proportional to the pulse width, picosecond pulses cannot provide a sufficiently broad range of measurements — picosecond frequency combs turn out to be too short. Sources of much shorter (femtosecond) laser pulses were needed to make frequency combs a practical tool for optical metrology. The advent of PCFs provided an opportunity to directly link such frequency combs to atomic frequency standards.

Convenient, reliable, and compact solid-state femtosecond laser systems, which became available in the early 1990s [30], can generate frequency combs with a bandwidth sufficient for practical applications in optical metrology and high-precision spectroscopy. The intermode interval $\Delta\omega$ can be locked to a radio-frequency reference source, such as, for example, an atomic cesium clock [81]. However, even with this task fulfilled, the frequency comb is still not fully linked to a reference frequency standard. The main source of difficulties lies in the fact that the frequency of the nth spectral component in the frequency comb is not an exact multiple of the intermode interval $\Delta\omega$ (see Fig. 15) but is given by the expression $\omega_n = n\Delta\omega + \omega_0$, where ω_0 is the offset frequency. One of the physical factors giving rise to this frequency offset is the dispersion of optical elements inside the laser cavity, making the phase velocity u_p of laser radiation different from the group velocity u_g of laser pulses. Because of the difference between u_p and u_g, the phase of the light field (the carrier phase) is systematically shifted relative to the pulse envelope from one pulse to another in a pulse train generated by a mode-locked laser. As a result, a femtosecond mode-locked laser delivers a sequence of pulses separated by equal time intervals T, but having a nonzero offset $\Delta\varphi$ of the carrier phase relative to the envelope phase. The Fourier transform of such a field gives a spectrum in the form of an equidistant comb of spectral components (see Fig. 15) with frequencies $\omega_n = n\Delta\omega + \omega_0$, where $\omega_0 = \Delta\varphi/T$.

To make a frequency comb suitable as a ruler for high-precision frequency measurements, the frequency ω_0 needs to be measured and stabilized relative to an external frequency standard. This problem is solved through supercontinuum

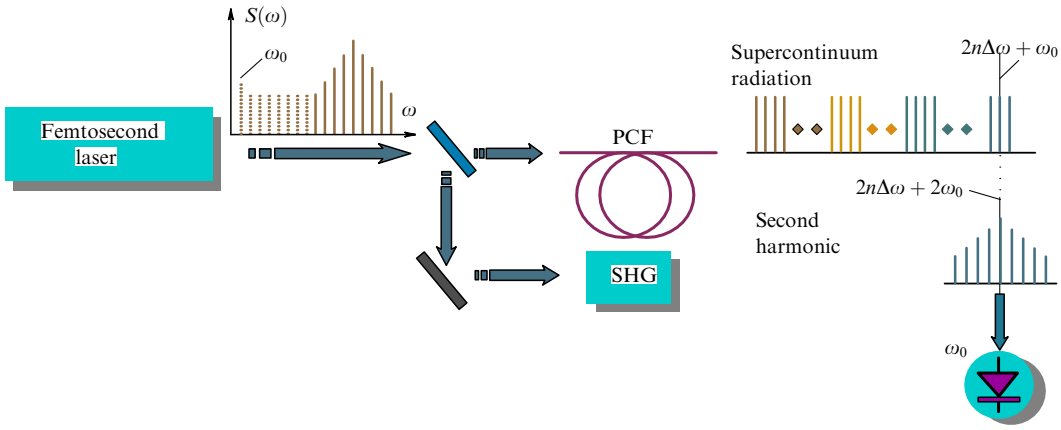

Figure 15. Measurement and stabilization of the carrier – envelope phase offset for a frequency comb generated by a mode-locked femtosecond laser.

generation in a PCF [78–80] or a tapered fiber [189, 190] (supercontinuum generation in tapered fibers involves the same physical scenarios as white-light generation in PCFs). The principle of ω_0 measurement and stabilization is illustrated in Fig. 15. A portion of a light beam produced by a femtosecond laser source of a frequency comb is coupled into a PCF. The remaining portion of the laser beam is frequency-doubled in a nonlinear crystal. The key requirement to supercontinuum generation in a PCF is that the spectrum of the supercontinuum at the output of the fiber should span an octave [81]. If this condition is satisfied, then, for any spectral component n picked from the low-frequency region of the frequency comb, the supercontinuum PCF output contains a frequency component $\omega_{2n} = 2n\Delta\omega + \omega_0$ close to the spectral component $2\omega_n = 2n\Delta\omega + 2\omega_0$ in the spectrum of the second harmonic from the nonlinear crystal (see Fig. 15). The beat signal produced by the second-harmonic field and the PCF output then contains a component $2\omega_n - \omega_{2n} = \omega_0$, allowing the offset frequency ω_0 to be measured and stabilized. This operation enables an accurate locking of all the spectral components in the femtosecond frequency comb with respect to a frequency standard using a single laser source.

Systems of optical metrology employing frequency combs can measure frequency intervals with a relative accuracy at a level of 5×10^{-16} [81]. The method of measurement and stabilization of the carrier–envelope phase offset, based on supercontinuum generation in a PCF, opens up the opportunity of the phase control of few-cycle laser pulses [191, 192]. Light pulses with a stabilized carrier–envelope phase offset are necessary for a controlled above-threshold ionization [193], high-order optical harmonic generation [194], and the generation of attosecond pulses [195]. Due to its simplicity, compactness, and reliability, the frequency-comb technique is gaining wide acceptance for the measurement of fundamental physical constants and the creation of practical optical-clock systems [81]. Applications of frequency-comb methods to satellite navigation and a high-precision synchronization of optical networks are also under consideration.

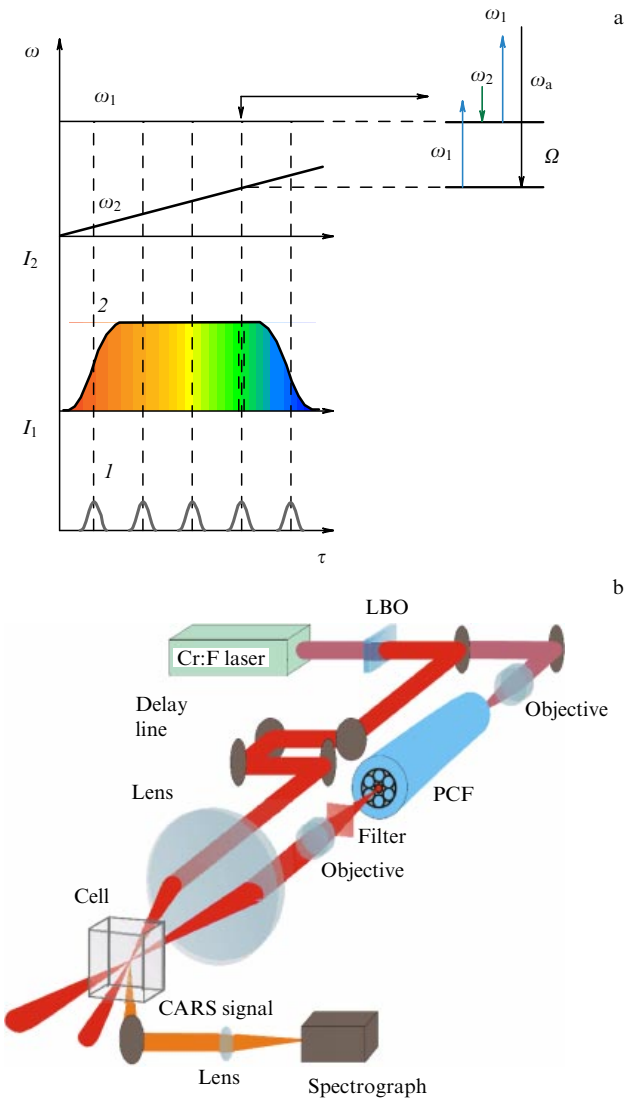

Figure 16. (a) Diagram of femtosecond CARS spectroscopy with chirped pulses. (b) A schematic of the experimental setup for CARS spectroscopy using a frequency-shifted chirped-pulse PCF output.

7.2 Fiber-optic white-light sources and frequency shifters in nonlinear spectroscopy

In this section we will discuss applications of PCF white-light sources and frequency shifters in nonlinear spectroscopy. We will show that spectral and temporal transformations of femtosecond laser pulses in PCFs with specifically designed dispersion profiles can deliver frequency tunable laser pulses with a tailored temporal intensity envelope and controlled chirp that are ideally suited to coherent Raman scattering and nonlinear absorption spectroscopy.

7.2.1 Coherent anti-Stokes Raman scattering spectroscopy. Coherent anti-Stokes Raman scattering [196, 197] is one of the most powerful and widespread techniques in nonlinear spectroscopy. CARS spectroscopy provides a high spatial, temporal, and spectral resolution [198] in the investigation of excited gas media, plasmas, flames, and combustion and offers new solutions for the coherent microscopy of biological objects [199] and ionized spatially nonuniform gas media [200]. Femtosecond CARS spectroscopy [201] gives access to ultrafast processes and the dynamics of vibrational wave packets in molecular systems residing in gas, liquid, or solid phases. Polarization [196, 198] and phase [202] control of four-wave mixing substantially enhances the potential of CARS spectroscopy and CARS microscopy, improving the sensitivity, as well as the temporal, spatial, and spectral resolutions of these methods.

The conceptual and technical progress of CARS spectroscopy has largely followed the development of tunable radiation sources. In many of the early CARS experiments, including the pioneering works on time-resolved CARS [203], the Stokes signal was generated through stimulated Raman scattering in a cell with a Raman-active gas. The advent of frequency-tunable light sources has opened a new phase in nonlinear spectroscopy [196]. Optical parametric oscillators and dye lasers have substantially expanded the area of application of CARS spectroscopy, allowing this technique to be employed, in particular, as a convenient and practical engineering tool for the diagnostics of combustion and flames in automobile and rocket engines [204, 205].

A new scheme of femtosecond CARS spectroscopy based on the use of chirped pulses was proposed and experimentally implemented in Refs [83, 206]. In this scheme, a variation in the delay time between a transform-limited pulse with a temporal intensity envelope $I_1(\tau)$ and a chirped pulse with a temporal envelope $I_2(\tau)$, as shown in Fig. 16a, scans the

instantaneous frequency difference $\omega_1 - \omega_2$ through Raman resonance. A linear time–frequency mapping defined by linearly chirped pulses thus allows the spectra of the nonlinear response of a medium to be measured by varying the delay time between the laser pulses [207, 208]. Photonic-crystal fibers with a special dispersion profile are at the heart of the experimental implementation of this technique. Such fibers are shown to be ideally suited for the generation of frequency-tunable pulses with a smooth temporal envelope and a controlled chirp. Due to the strong confinement of electromagnetic radiation in the fiber core and the possibility of tailoring the dispersion of guided modes, PCFs can radically enhance nonlinear-optical frequency conversion of femtosecond pulses, opening up opportunities for the creation of conceptually new sources of frequency-tunable radiation for nonlinear spectroscopy. In the experiments discussed below in this section, femtosecond pulses that are frequency-upconverted and shaped in PCFs are employed for the CARS spectroscopy of toluene molecules in solution.

The laser system employed in experiments [83, 206] consisted of a Cr^{4+}:forsterite master oscillator, a stretcher, an optical isolator, a regenerative amplifier, a compressor, and a nonlinear crystal for frequency doubling [155] (Fig. 16b). The master oscillator, pumped with an ytterbium fiber laser, generated 30–50-fs light pulses with a repetition rate of 120 MHz. The central wavelength of this laser radiation was approximately equal to 1270 nm with a bandwidth of 26 nm and a mean power of about 180 mW. These horizontally polarized 30–50-fs pulses were stretched up to 700 ps in a grating stretcher and then amplified in an Nd:YLF-laser-pumped regenerative amplifier. Amplified pulses with an energy up to 100 μJ were recompressed to a 75–150-fs duration in a grating compressor. Approximately 50% of the pulse energy was lost at this stage. An LBO crystal was employed for the frequency doubling of the fundamental-wavelength femtosecond pulses of the Cr:forsterite laser.

Photonic-crystal fibers employed in our experiments were fabricated from multicomponent glass. The fiber structure (see the inset to Fig. 16b) was designed in such a way as to provide the optimal dispersion profile for the maximum efficiency of dispersive-wave emission in the anti-Stokes wavelength range from 650 to 730 nm by solitons excited with femtosecond Cr:forsterite-laser pulses.

Cross-correlation frequency-resolved optical gating (XFROG) [209–211] was applied to measuring the spectrum and the temporal envelope of the frequency-shifted PCF output. An XFROG signal was generated by mixing the anti-Stokes-shifted PCF output, E_a, with the second-harmonic output of the Cr:forsterite laser, E_{SH}, in a BBO crystal. A two-dimensional XFROG spectrogram, namely

$$S(\omega, \tau) \propto \left| \int_{-\infty}^{\infty} E_a(t)\, E_{SH}(t - \tau) \exp(-i\omega t)\, dt \right|^2,$$

was then plotted in the standard way by measuring the XFROG signal as a function of the delay time τ between the second-harmonic and PCF-output pulses and spectrally dispersing the XFROG signal. The XFROG sonogram visualizes the temporal envelope, the spectrum, and the chirp of the PCF output. Figure 17a portrays an XFROG spectrogram of the PCF output measured with the use of 620-nm 90-fs second-harmonic pulses. As can be seen from this map, the PCF output has a pulse width of about 1 ps, a smooth temporal envelope, and a virtually linear positive chirp.

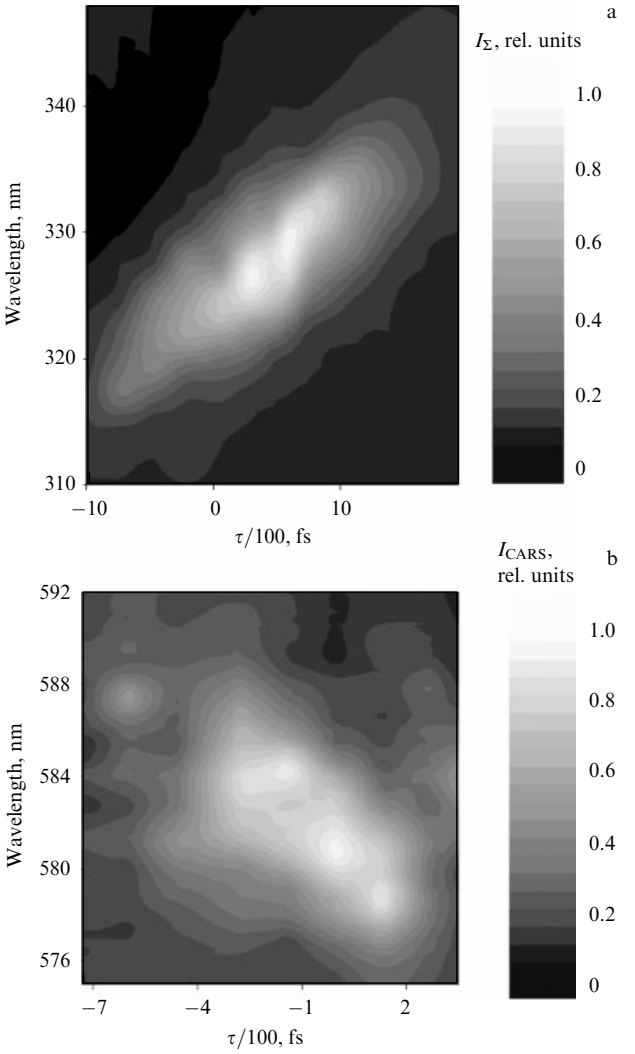

Figure 17. (a) The intensity I_Σ of the sum-frequency signal generated in a BBO crystal by the second-harmonic pulse from a Cr:forsterite laser and the anti-Stokes-shifted PCF output as a function of the wavelength and the delay time τ between the second-harmonic and PCF-output pulses. (b) The intensity I_{CARS} of the CARS signal generated in a noncoplanar boxcars geometry from a toluene solution as a function of the wavelength and the delay time τ between the second-harmonic and PCF-output pulses.

Different frequency components of the anti-Stokes-shifted PCF output are characterized by different group delays. The instantaneous frequency ω in this pulse, as can be seen from the measured results presented in Fig. 17a, is related to the delay time τ by a one-to-one mapping determined by the chirp. Such a one-to-one $\tau \leftrightarrow \omega$ mapping allows spectral measurements to be performed by varying the delay time between the PCF output and a fixed-frequency pump pulse. In our experiments, we used the linearly chirped anti-Stokes-shifted PCF output as one of the biharmonic pump fields for the CARS spectroscopy of a toluene solution.

Second-harmonic pulses of the Cr:forsterite laser (the frequency ω_1) and the anti-Stokes PCF output (the frequency ω_2) were employed in our CARS scheme to coherently excite Raman-active modes of toluene molecules with a frequency $\Omega = \omega_1 - \omega_2$ in solution. The second-harmonic field of the Cr:forsterite laser (the probe pulse) is then

scattered off the coherence prepared in the medium by the first two pulses, generating the CARS signal at the frequency $\omega_{CARS} = 2\omega_1 - \omega_2$. The PCF structure was optimized for efficient frequency conversion of Cr:forsterite laser pulses to the wavelength range allowing Raman-active modes of toluene molecules to be probed within the range of wavenumbers from 1000 up to 1200 cm^{-1}. Light beams with frequencies ω_1 and ω_2 were focused into a cell with a toluene solution at a small angle with respect to each other (Fig. 16b). The CARS signal generated in the area of beam interaction in this noncoplanar boxcars geometry had the form of a sharply directed light beam with a low, phase-matching-controlled angular divergence, being spatially separated from the laser and PCF output beams. This signal was then filtered and detected with a spectrometer.

Figure 17b displays an XFROG CARS spectrogram of Raman-active modes of toluene. The frequency difference $\omega_1 - \omega_2$ was scanned through the frequencies of the Raman-active modes of toluene molecules by tuning the delay time τ between the second-harmonic output of the Cr:forsterite laser and the anti-Stokes-shifted PCF output. In the positively chirped pulse from the microstructure fiber, the instantaneous frequency increases from the leading to the trailing edge (see Fig. 17a). Small delay times τ, therefore, correspond to the excitation of low-frequency Raman-active modes ($\tau \approx -200$ fs in Fig. 17b). In particular, the 1004-cm^{-1} Raman mode of toluene molecule is well-resolved in the presented XFROG CARS spectrogram. This mode is excited with the second harmonic of Cr:forsterite-laser radiation and the spectral slice around the wavelength $\lambda_2 \approx 661$ nm picked with an appropriate delay time from the positively chirped PCF output, giving rise to a CARS signal with the wavelength $\lambda_{CARS} \approx 584$ nm. Raman modes with higher frequencies are probed with larger delay times ($\tau \approx 100-200$ fs in Fig. 17b), with larger frequency differences $\omega_1 - \omega_2$ leading to the generation of a higher-frequency CARS signal.

7.2.2 Nonlinear absorption spectroscopy. Time-resolved nonlinear-optical spectroscopy of molecular dynamics and fast excitation-transfer processes typically involves specifically designed sequences of pump and probe light pulses with a variable delay time and a smoothly tunable frequency of the probe field [201]. In a laboratory experiment, such pulse sequences can be generated by femtosecond optical parametric amplifiers (OPAs). Femtosecond OPAs, however, inevitably increase the cost of laser experiments and make the laser system more complicated, unwieldy, expensive, and difficult to align.

An interesting alternative strategy of pump–probe spectroscopy employs a pump field in the form of a broadband, e.g., supercontinuum, radiation with a precisely characterized chirp [207, 208, 212, 213]. The supercontinuum probe pulse for pump–probe experiments is often generated by focusing amplified femtosecond pulses into a silica or sapphire plate [26, 212, 213]. Photonic-crystal fibers can generate supercontinuum probe pulses with a tunable frequency, tailored temporal envelope, and controlled phase, suggesting interesting new options for time-resolved nonlinear spectroscopy.

Figure 18 illustrates the concept of time-resolved nonlinear absorption spectroscopy of molecular aggregates with the aid of a femtosecond pump pulse and a broadband chirped probe pulse delivered and shaped by a PCF [214]. Experiments were performed with thiacarbocyanine molecular aggregates in a polymer film. Polymer materials doped with molecular aggregates offer much promise as novel media for nonlinear optics and ultrafast photonics, allowing the creation of efficient switches and limiters for ultrashort laser pulses [215].

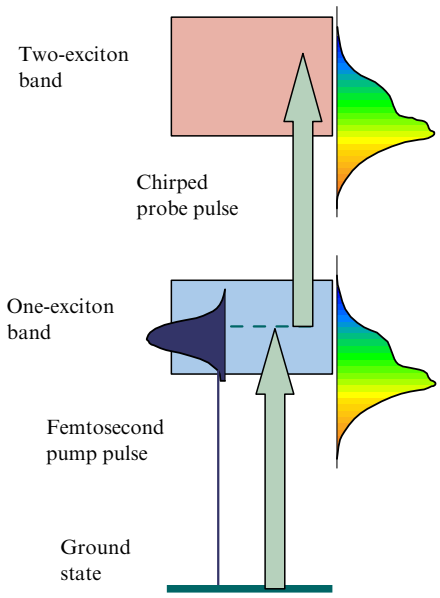

Figure 18. A schematic of time-resolved pump–probe nonlinear-absorption spectroscopy of exciton bands in molecular aggregates using a femtosecond pump pulse and a broadband chirped probe field.

Collective electronic eigenstates in aggregates of strongly coupled molecules are grouped into excitonic bands (see Fig. 18). The widths of excitonic bands and their shifts with respect to the energy levels of noninteracting molecules can provide important information on the character and strength of intermolecular interactions in aggregates, often allowing an estimation of the number of molecules forming an aggregate.

Nonlinear absorption spectroscopy provides a convenient tool for studying exciton energy bands of molecular aggregates and for measuring their parameters (see Fig. 18). In experiments [214], the second-harmonic output of a Cr:forsterite laser with a central wavelength of 618 nm, a pulse width of about 120 fs, and an energy ranging from 10 to 80 nJ was used as a pump field. Frequency-tunable upconversion of fundamental-wavelength Cr:forsterite-laser pulses was performed through the nonlinear-optical spectral transformation of these pulses in a multicomponent-glass PCF with the cross-section structure shown in the inset to Fig. 12a. The dispersion profile of this PCF provided an efficient transformation of femtosecond Cr:forsterite-laser pulses into a broadband signal with spectrum stretching (at the level of 20% of its maximum) from 530 to 680 nm. This blue-shifted PCF output was used as a probe field for measuring the pump-induced absorption spectrum of molecular aggregates.

Figure 19 portrays the spectra of differential absorption, obtained by subtracting absorption spectra measured in the absence of the Cr:forsterite pump pulse from the absorption spectra measured in the presence of the pump pulse. Nonlinear absorption spectra shown in Fig. 19 display well-pronounced minima at 665 nm and blue-shifted peaks at 640 nm. Such features are typical of nonlinear absorption

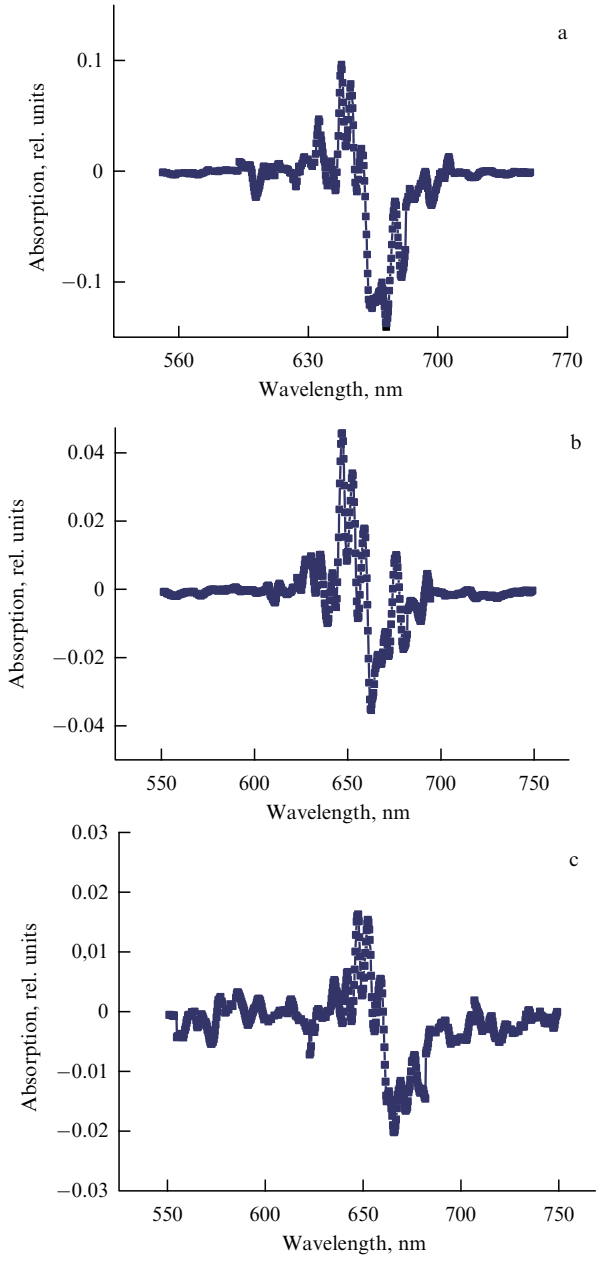

Figure 19. Differential spectra of nonlinear absorption measured by the pump – probe technique for thiacarbocyanine molecular aggregates in a polymer film with a delay time between the probe and pump pulses equal to (a) 100 fs, (b) 500 fs, and (c) 1100 fs.

spectra of J-type molecular aggregates, measured by the pump – probe technique [215]. The negative feature is indicative of bleaching through pump-induced transitions between the ground state and the one-exciton band, while the blue-shifted peak originates from induced absorption due to transitions between one- and two-exciton bands of molecular aggregates.

For highly ordered aggregates, the spectrum of nonlinear absorption is dominated by transitions between the ground state and lowest one- and two-exciton bands [216, 217]. The exciton delocalization length can then be estimated from the spectral shift Δ of the induced-absorption peak relative to the bleaching minimum using the following formula [218, 219]: $N_{\rm d}^{\Delta} \approx (3\pi^2|J|/\Delta)^{1/2} - 1$. With the spectral shift estimated as $\Delta \approx 470$ cm^{-1} [214], we find that $N_{\rm d}^{\Delta} \approx 6$, in perfect agreement with the value of delocalization length obtained from aggregate absorption spectra.

The amplitudes of both positive and negative features in nonlinear absorption spectra decay on a subpicosecond time scale with increasing delay time between the pump and probe pulses (cf. Figs 19a – c), indicating a subpicosecond relaxation rate of the one-exciton state of molecular aggregates. This finding suggests, in agreement with earlier studies of ultrafast excitation-energy transfer processes in molecular aggregates, that the relaxation dynamics of aggregates in our experimental conditions is mainly controlled by the quenching of excited states of aggregates through exciton – exciton annihilation [215].

Experiments discussed in this section reveal that PCFs with a specially designed dispersion offer ways of creating efficient sources of ultrashort pulses for coherent nonlinear spectroscopy. These fibers provide a high efficiency of frequency up-conversion of nano- and subnanojoule femtosecond laser pulses, permitting the generation of blue-shifted pulses with a tailored temporal envelope, controlled spectral properties, and an optimized chirp [220]. Photonic-crystal fibers thus allow the creation of tunable light sources for nonlinear spectroscopy and quantum control, with requirements to the pump energy substantially loosened relative to dye lasers and optical parametric amplifiers. The peak power of the frequency-shifted PCF output can be radically increased by means of optical parametric amplification [221] or through laser amplification followed by optical parametric amplification [159].

8. Conclusion

Nonlinear-optical interactions of ultrashort laser pulses can efficiently generate an artificial white light with unique spectral properties, a controlled pulse duration, a tailored temporal envelope, and a high spectral brightness. Materials and structures allowing an efficient transformation of ultrashort laser pulses into supercontinuum radiation offer new solutions for optical communications and ultrafast optics. Supercontinuum generators based on photonic-crystal fibers help achieve an unprecedented precision in optical metrology and suggest new strategies for the creation of compact multiplex light sources for nonlinear spectroscopy, microscopy, and laser biomedicine. Analysis of supercontinuum generation in PCFs reveals new regimes of nonlinear-optical interactions of ultrashort laser pulses. Novel fiber-optic structures and materials with high optical nonlinearities provide high efficiencies of spectral and temporal transformations of ultrashort laser pulses, permitting the generation of broadband field waveforms with controlled spectral, temporal, and phase parameters.

Acknowledgments

I am pleased to gratefully acknowledge fruitful collaboration and illuminating discussions with A B Fedotov, D A Sidorov-Biryukov, E E Serebryannikov, and D A Akimov (Physics Department, M V Lomonosov Moscow State University); A A Ivanov and M V Alfimov (Center of Photochemistry, Russian Academy of Sciences); R Miles (Princeton University); A Baltuška and F Krausz (Max Planck Institute for Quantum Optics, Garching); D von der Linde and A P Tarasevitch (University of Essen – Duisburg); W Kiefer (Würzburg University); P St J Russell, D Skryabin, and J Knight (University of Bath); Yu N Kondrat'ev, V S Shevan-

din, K V Dukel'skii, and A V Khokhlov (S I Vavilov State Optical Institute, St.-Petersburg); V I Beloglazov, N B Skibina, and A V Shcherbakov (Institute of Technology and Equipment for Glass Structures, Saratov); G Stegeman and R Stegeman (University of Central Florida); D Chorvat and I Bugar (International Laser Center, Bratislava); J Dudley (University of Besancon); C Sibilia (La Sapienza University of Rome); Ching-yue Wang, Minglie Hu, and Yanfeng Li (Tianjin University), and L A Mel'nikov (N G Chernyshevsky Saratov State University).

This study was supported in part by the Russian Foundation for Basic Research (project Nos 03-02-16929, 03-02-20002-BNTS-a, and 05-02-90566-NNS), the Russian Federal Research and Technology Program (contract No. 02.434.11.2010), and INTAS (project Nos 03-51-5037 and 03-51-5288). The research described in this publication was made possible in part by Award No. RP2-2558 of the U.S. Civilian Research & Development Foundation for the Independent States of the Former Soviet Union (CRDF).

References

1. *Oeuvres de Descartes* (Paris: Charles Adam et Paul Tannery, 1902) [Translated into Russian (Moscow: Gospolitizdat, 1950)]
2. Grimaldi F M *Physico-mathesis de lumine, coloribus et iride* (Bologna: A. Forni, 1665)
3. Newton I *Optics* (London: Smith & Walford, 1704) [Translated into Russian (Moscow – Leningrad: Izd. Akad. Nauk SSSR, 1954)]
4. Raman C V, Krishnan K S *Nature* **121** 501 (1928)
5. Landsberg G, Mandelstam L *Naturwissenschaften* **16** 557 (1928)
6. Placzek G, in Rayleigh-Streuung und Raman-Effekt (Handbuch der Radiologie, 2 Auflage, Bd. 6, Pt. II, Ed. G Marx) (Leipzig: Akademische Verlagsgesellschaft, 1934) p. 205 [Translated into English: *The Rayleigh and Raman Scattering* (Washington, DC: US Dept. Commerce, 1934); translated into Russian (Khar'kov: ONTIU, 1934)]
7. Fabelinskii I L *Molekulyarnoe Rasseyanie Sveta* (Molecular Scattering of Light) (Moscow: Nauka, 1965) [Translated into English (New York: Plenum Press, 1968)]
8. Fabelinskiĭ I L *Usp. Fiz. Nauk* **168** 1341 (1998) [*Phys. Usp.* **41** 1229 (1998)]
9. The Nobel Prize in Physics 2005, http://nobelprize.org/physics/laureates/2005/index.html
10. Alfano R R, Shapiro S L *Phys. Rev. Lett.* **24** 584 (1970)
11. Alfano R R, Shapiro S L *Phys. Rev. Lett.* **24** 592 (1970)
12. Yu W et al. *Opt. Commun.* **14** 344 (1975)
13. Werncke W et al. *Opt. Commun.* **4** 413 (1972)
14. Penzkofer A, Laubereau A, Kaiser W *Phys. Rev. Lett.* **31** 863 (1973)
15. Smith W L, Liu P, Bloembergen N *Phys. Rev. A* **15** 2396 (1977)
16. Fork R L et al. *Opt. Lett.* **8** 1 (1983)
17. Corkum P B, Rolland C, Srinivasan-Rao T *Phys. Rev. Lett.* **57** 2268 (1986)
18. Glownia J H, Misewich J, Sorokin P P *J. Opt. Soc. Am. B* **3** 1573 (1986)
19. Lin C, Stolen R H *Appl. Phys. Lett.* **28** 216 (1976)
20. Baldeck P L, Alfano R R *J. Lightwave Technol.* **5** 1712 (1987)
21. Yang G, Shen Y R *Opt. Lett.* **9** 510 (1984)
22. Becker P C et al. *Appl. Phys. Lett.* **54** 411 (1989)
23. Schoenlein R W et al. *Appl. Phys. Lett.* **58** 801 (1991)
24. Nisoli M, De Silvestri S, Svelto O *Appl. Phys. Lett.* **68** 2793 (1996)
25. Morioka T, Mori K, Saruwatari M *Electron. Lett.* **29** 862 (1993)
26. Alfano R R (Ed.) *The Supercontinuum Laser Source* (New York: Springer-Verlag, 1989)
27. Zheltikov A M (Ed.) "Supercontinuum generation: Special issue" *Appl. Phys. B* **77** (2/3) (2003)
28. Shen Y R *The Principles of Nonlinear Optics* (New York: J. Wiley, 1984) [Translated into Russian (Moscow: Nauka, 1989)]
29. Akhmanov S A, Vysloukh V A, Chirkin A S *Optika Femtosekundnykh Lazernykh Impul'sov* (Optics of Femtosecond Laser Pulses) (Moscow: Nauka, 1988) [Translated into English (New York: American Institute of Physics, 1992)]
30. Brabec T, Krausz F *Rev. Mod. Phys.* **72** 545 (2000)
31. Akhmanov S A, Sukhorukov A P, Khokhlov R V *Usp. Fiz. Nauk* **93** 19 (1967) [*Sov. Phys. Usp.* **10** 609 (1968)]
32. Agrawal G P *Nonlinear Fiber Optics* 3rd ed. (San Diego, CA: Academic Press, 2001)
33. Gustafson T K et al. *Phys. Rev.* **177** 306 (1969)
34. Corkum P B, Rolland C *IEEE J. Quantum Electron.* **25** 2634 (1989)
35. Bloembergen N *Opt. Commun.* **8** 285 (1973)
36. Ilkov F A, Ilkova L Sh, Chin S L *Opt. Lett.* **18** 681 (1993)
37. Braun A et al. *Opt. Lett.* **20** 73 (1995)
38. Nibbering E T J et al. *Opt. Lett.* **21** 62 (1996)
39. Brodeur A et al. *Opt. Lett.* **22** 304 (1997)
40. Nishioka H et al. *Opt. Lett.* **20** 2505 (1995)
41. La Fontaine B et al. *Phys. Plasmas* **6** 1615 (1999)
42. Tzortzakis S et al. *Opt. Lett.* **25** 1270 (2000)
43. Mlejnek M, Wright E M, Moloney J V *Opt. Lett.* **23** 382 (1998)
44. Chiron A et al. *Eur. Phys. J. D* **6** 383 (1999)
45. Kandidov V P et al. *Appl. Phys. B* **77** 149 (2003)
46. Rairoux P et al. *Appl. Phys. B* **71** 573 (2000)
47. Kasparian J et al. *Opt. Lett.* **25** 1397 (2000)
48. Méjean G et al. *Appl. Phys. B* **77** 357 (2003)
49. Gaeta A L *Phys. Rev. Lett.* **84** 3582 (2000)
50. Aközbek N et al. *Opt. Commun.* **191** 353 (2001)
51. Nibbering E T J et al. *J. Opt. Soc. Am. B* **14** 650 (1997)
52. Blow K J, Wood D *IEEE J. Quantum Electron.* **25** 2665 (1989)
53. Brodeur A, Chin S L *Phys. Rev. Lett.* **80** 4406 (1998)
54. Brodeur A, Chin S L *J. Opt. Soc. Am. B* **16** 637 (1999)
55. Liu W et al. *Opt. Commun.* **202** 189 (2002)
56. Smith W L, Liu P, Bloembergen N *Phys. Rev. A* **15** 2396 (1977)
57. Kolesik M et al. *Phys. Rev. Lett.* **91** 043905 (2003)
58. Tamura K R, Kubota H, Nakazawa M *IEEE J. Quantum Electron.* **36** 773 (2000)
59. Sotobayashi H, Kitayama K *Electron. Lett.* **34** 1336 (1998)
60. Russell P *Science* **299** 358 (2003)
61. Knight J C *Nature* **424** 847 (2003)
62. Zheltikov A M *Optika Mikrostrukturirovannykh Volokon* (Optics of Photonic-Crystal Fibers) (Moscow: Nauka, 2004)
63. Knight J C et al. *Opt. Lett.* **21** 1547 (1996)
64. Bjarklev A, Broeng J, Bjarklev A S *Photonic Crystal Fibers* (Boston: Kluwer Acad. Publ., 2003)
65. Knight J C et al. *Science* **282** 1476 (1998)
66. Cregan R F et al. *Science* **285** 1537 (1999)
67. Konorov S O et al. *Pis'ma Zh. Eksp. Teor. Fiz.* **76** 401 (2002) [*JETP Lett.* **76** 341 (2002)]
68. Smith C M et al. *Nature* **424** 657 (2003)
69. Marcatili E A J, Schmeltzer R A *Bell Syst. Tech. J.* **43** 1783 (1964)
70. Adams M J *An Introduction to Optical Waveguides* (New York: Wiley, 1981)
71. Bowden C M, Zheltikov A M (Eds) "Nonlinear optics of photonic crystals: Feature issue" *J. Opt. Soc. Am. B* **19** (9) (2002)
72. Zheltikov A M *Usp. Fiz. Nauk* **174** 73 (2004) [*Phys. Usp.* **47** 69 (2004)]
73. Ferrando A et al. *Opt. Lett.* **25** 790 (2000)
74. Reeves W H et al. *Nature* **424** 511 (2003)
75. Fedotov A B et al. *Appl. Phys. B* **73** 181 (2001)
76. Ranka J K, Windeler R S, Stentz A J *Opt. Lett.* **25** 25 (2000)
77. Wadsworth W J et al. *J. Opt. Soc. Am. B* **19** 2148 (2002)
78. Jones D J et al. *Science* **288** 635 (2000)
79. Holzwarth R et al. *Phys. Rev. Lett.* **85** 2264 (2000)
80. Diddams S A et al. *Phys. Rev. Lett.* **84** 5102 (2000)
81. Udem Th, Holzwarth R, Hänsch T W *Nature* **416** 233 (2002)
82. Hartl I et al. *Opt. Lett.* **26** 608 (2001)
83. Konorov S O et al. *Phys. Rev. E* **70** 057601 (2004)
84. Konorov S O et al. *Chem. Phys. Lett.* **405** 310 (2005)
85. Paulsen H N et al. *Opt. Lett.* **28** 1123 (2003)
86. Konorov S, Zheltikov A *Opt. Express* **11** 2440 (2003)
87. Sharping J et al. *Opt. Express* **12** 3086 (2004)
88. Rarity J et al. *Opt. Express* **13** 534 (2005)
89. Baltuska A, Fuji T, Kobayashi T *Opt. Lett.* **27** 1241 (2002)
90. Coen S et al. *J. Opt. Soc. Am. B* **19** 753 (2002)
91. Dudley J M et al. *J. Opt. Soc. Am. B* **19** 765 (2002)
92. Nikolov N I et al. *J. Opt. Soc. Am. B* **20** 2329 (2003)
93. Akimov D A et al. *Opt. Lett.* **28** 1948 (2003)
94. Ortigosa-Blanch A et al. *Opt. Lett.* **25** 1325 (2000)
95. Steel M J, Osgood R M (Jr) *Opt. Lett.* **26** 229 (2001)

96. Hansen T P et al. *IEEE Photon. Technol. Lett.* **13** 588 (2001)
97. Apolonski A et al. *J. Opt. Soc. Am. B* **19** 2165 (2002)
98. Lehtonen M et al. *Appl. Phys. Lett.* **82** 2197 (2003)
99. Hu M et al. *Opt. Express* **12** 1932 (2004)
100. Szpuliak A et al. *J. Opt. Soc. Am. B* (in press)
101. Hu M et al. *Opt. Express* **13** 5947 (2005)
102. Furusawa K et al. *Opt. Express* **9** 714 (2001)
103. Wadsworth W et al. *Opt. Express* **11** 48 (2003)
104. Pickrell G, Peng W, Wang A *Opt. Lett.* **29** 1476 (2004)
105. Jensen J B et al. *Opt. Lett.* **29** 1974 (2004)
106. Konorov S, Zheltikov A, Scalora M *Opt. Express* **13** 3454 (2005)
107. Benabid F et al. *Science* **298** 399 (2002)
108. Zheltikov A M *Usp. Fiz. Nauk* **174** 1301 (2004) [*Phys. Usp.* **47** 1205 (2004)]
109. Benabid F et al. *Nature* **434** 488 (2005)
110. Konorov S O, Fedotov A B, Zheltikov A M *Opt. Lett.* **28** 1448 (2003)
111. Konorov S O et al. *Phys. Rev. E* **70** 066625 (2004)
112. Fedotov A B et al. *Phys. Rev. A* **70** 045802 (2004)
113. Konorov S O et al. *Phys. Rev. E* **71** 057603 (2005)
114. Konorov S O et al. *Appl. Phys. Lett.* **85** 3690 (2004)
115. Ouzounov D et al. *Opt. Express* **13** 6153 (2005)
116. Zheltikova D A et al. *Phys. Rev. E* **71** 026609 (2005)
117. Konorov S O et al. *Phys. Rev. A* **70** 023807 (2004)
118. Konorov S O et al. *Appl. Phys. B* **78** 547 (2004)
119. Konorov S O et al. *J. Phys. D*: *Appl. Phys.* **36** 1375 (2003)
120. Shephard J et al. *Opt. Express* **12** 717 (2004)
121. Konorov S O et al. *Appl. Opt.* **43** 2251 (2004)
122. Ouzounov D G et al. *Science* **301** 1702 (2003)
123. Luan F et al. *Opt. Express* **12** 835 (2004)
124. Konorov S O et al. *Opt. Lett.* **29** 1521 (2004)
125. Zheltikov A M *Nature Mater.* **4** 267 (2005)
126. Zheltikova D A, Zheltikov A M *Appl. Phys B* (in press)
127. Zheltikov A M (Ed.) ''Photonic crystals: Special issue'' *Appl. Phys. B* **81** (2/3) (2005)
128. Skryabin D V et al. *Science* **301** 1705 (2003)
129. Zheltikov A M *Phys. Rev. A* **72** 043812 (2005); *J. Opt. Soc. Am. B* **22** 2263 (2005)
130. Konorov S O et al. *Appl. Phys. B* **81** 219 (2005)
131. Harvey J D et al. *Opt. Lett.* **28** 2225 (2003)
132. Hu M et al. *Appl. Phys. B* **79** 805 (2004)
133. Dianov E M et al. *Pis'ma Zh. Eksp. Teor. Fiz.* **41** 242 (1985) [*JETP Lett.* **41** 294 (1985)]
134. Mitschke F M, Mollenauer L F *Opt. Lett.* **11** 659 (1986)
135. Wai P K A, Chen H H, Lee Y C *Phys. Rev. A* **41** 426 (1990)
136. Akhmediev N, Karlsson M *Phys. Rev. A* **51** 2602 (1995)
137. Ranka J K, Windeler R S, Stentz A J *Opt. Lett.* **25** 796 (2000)
138. Omenetto F G et al. *Opt. Lett.* **26** 1158 (2001)
139. Omenetto F et al. *Opt. Express* **11** 61 (2003)
140. Efimov A et al. *Opt. Express* **11** 910 (2003)
141. Efimov A et al. *Opt. Express* **11** 2567 (2003)
142. Naumov A N et al. *J. Opt. Soc. Am. B* **19** 2183 (2002)
143. Akimov D A et al. *Appl. Phys. B* **76** 515 (2003)
144. Whitham G B *Proc. R. Soc. London Ser. A* **283** 238 (1965)
145. Bespalov V I, Talanov V I *Pis'ma Zh. Eksp. Teor. Fiz.* **3** 471 (1966) [*JETP Lett.* **3** 307 (1966)]
146. Taniuti T, Washimi H *Phys. Rev. Lett.* **21** 209 (1968)
147. Salasnich L, Parola A, Reatto L *Phys. Rev. Lett.* **91** 080405 (2003)
148. Malendevich R et al. *Opt. Lett.* **26** 1879 (2001)
149. Tai K, Hasegawa A, Tomita A *Phys. Rev. Lett.* **56** 135 (1986)
150. Sharping J E et al. *Opt. Lett.* **27** 1675 (2002)
151. Fedotov A B et al. *Opt. Commun.* **255** 218 (2005)
152. Serebryannikov E E et al. *Phys. Rev. E* **72** 027601 (2005)
153. Agrawal G P *Phys. Rev. Lett.* **59** 880 (1987)
154. Monro T M et al. *J. Lightwave Technol.* **18** 50 (2000)
155. Ivanov A A, Alfimov M V, Zheltikov A M *Usp. Fiz. Nauk* **174** 743 (2004) [*Phys. Usp.* **47** 687 (2004)]
156. Liu X et al. *Opt. Lett.* **26** 358 (2001)
157. Serebryannikov E E et al. *Appl. Phys. B* **81** 585 (2005)
158. Serebryannikov E E et al. *Phys. Rev. E* **72** 056603 (2005)
159. Teisset C et al. *Opt. Express* **13** 6550 (2005)
160. Gordon J P *Opt. Lett.* **11** 662 (1986)
161. Serebryannikov E E et al. *Pis'ma Zh. Eksp. Teor. Fiz.* **81** 605 (2005) [*JETP Lett.* **81** 487 (2005)]
162. Stolen R H et al. *J. Opt. Soc. Am. B* **6** 1159 (1989)
163. Serebryannikov E E, Zheltikov A M *J. Opt. Soc. Am. B* (in press)
164. Serebryannikov E E et al. *Phys. Rev. E* (in press)
165. Mamyshev P V, Chernikov S V *Opt. Lett.* **15** 1076 (1990)
166. Kibler B, Dudley J M, Coen S *Appl. Phys. B* **81** 337 (2005)
167. Santhanam J, Agrawal G P *Opt. Commun.* **222** 413 (2003)
168. Herrmann J et al. *Phys. Rev. Lett.* **88** 173901 (2002)
169. Biancalana F, Skryabin D V, Yulin A V *Phys. Rev. E* **70** 016615 (2004)
170. Friberg S, Smith P *IEEE J. Quantum Electron.* **23** 2089 (1987)
171. Petropoulos P et al. *Opt. Express* **11** 3568 (2003)
172. Kanth Kumar V V R et al. *Opt. Express* **10** 1520 (2002)
173. Hundertmark H et al. *Opt. Express* **11** 3196 (2003)
174. Okuno T et al. *IEEE J. Sel. Top. Quantum Electron.* **5** 1385 (1999)
175. Nicholson J W et al. *Opt. Lett.* **28** 643 (2003)
176. Kanth Kumar V V R et al. *Opt. Express* **11** 2641 (2003)
177. Slusher R E et al. *J. Opt. Soc. Am. B* **21** 1146 (2004)
178. Thielen P A et al. *Opt. Lett.* **28** 1406 (2003)
179. Monro T M et al. *Electron. Lett.* **36** 1998 (2000)
180. Konorov S et al. *Opt. Express* **13** 5682 (2005)
181. Stegeman R et al. *Opt. Lett.* **28** 1126 (2003)
182. Stegeman R et al. *J. Opt. Soc. Am. B* **22** 1861 (2005)
183. Serebryannikov E E, Rivero C, Stegeman R, Zheltikov A M (submitted)
184. Reichert J et al. *Opt. Commun.* **172** 59 (1999)
185. Udem Th et al. *Opt. Lett.* **24** 881 (1999)
186. Udem Th et al. *Phys. Rev. Lett.* **82** 3568 (1999)
187. Eckstein J N, Ferguson A I, Hänsch T W *Phys. Rev. Lett.* **40** 847 (1978)
188. Baklanov Ye V, Chebotayev V P *Appl. Phys.* **12** 97 (1977)
189. Birks T A, Wadsworth W J, Russell P St J *Opt. Lett.* **25** 1415 (2000)
190. Bagayev S N et al. *Laser Phys.* **11** 1270 (2001)
191. Apolonski A et al. *Phys. Rev. Lett.* **85** 740 (2000)
192. Telle H R et al. *Appl. Phys. B* **69** 327 (1999)
193. Paulus G G et al. *Nature* **414** 182 (2001)
194. Drescher M et al. *Science* **291** 1923 (2001)
195. Baltuška A et al. *Nature* **421** 611 (2003)
196. Akhmanov S A, Koroteev N I *Metody Nelineinoi Optiki v Spektroskopii Rasseyaniya Sveta* (Methods of Nonlinear Optics in Light Scattering Spectroscopy) (Moscow: Nauka, 1981)
197. Eesley G L *Coherent Raman Spectroscopy* (Oxford: Pergamon Press, 1981)
198. Zheltikov A M, Koroteev N I *Usp. Fiz. Nauk* **169** 385 (1999) [*Phys. Usp.* **42** 321 (1999)]
199. Zumbusch A, Holtom G R, Sunney Xie X *Phys. Rev. Lett.* **82** 4142 (1999)
200. Akimov D A et al. *Proc. SPIE* **4749** 101 (2002)
201. Kiefer W (Ed.) ''Femtosecond coherent Raman spectroscopy: Special issue'' *J. Raman Spectrosc.* **31** (1/2) (2000)
202. Dudovich N, Oron D, Silberberg Y *Nature* **418** 512 (2002)
203. von der Linde D, Laubereau A, Kaiser W *Phys. Rev. Lett.* **26** 954 (1971)
204. Radi P, Zheltikov A (Eds) ''Nonlinear Raman spectroscopy: Special issue'' *J. Raman Spectrosc.* **33** (11/12) (2002)
205. Radi P, Zheltikov A M (Eds) "Nonlinear Raman spectroscopy: Special issue" *J. Raman Spectrosc.* **34** (12) (2003)
206. Konorov S O et al. *Appl. Phys. B* **78** 565 (2004)
207. Naumov A N, Zheltikov A M *J. Raman Spectrosc.* **32** 960 (2001)
208. Naumov A N, Zheltikov A M *Appl. Phys. B* **77** 369 (2003)
209. Linden S, Kuhl J, Giessen H *Opt. Lett.* **24** 569 (1999)
210. Gu X et al. *Opt. Lett.* **27** 1174 (2002)
211. Trebino R *Frequency-Resolved Optical Gating*: *The Measurement of Ultrashort Laser Pulses* (Boston: Kluwer Acad., 2002)
212. Kovalenko S A et al. *Phys. Rev. A* **59** 2369 (1999)
213. Lang T, Motzkus M *J. Opt. Soc. Am. B* **19** 340 (2002)
214. Ivanov A A et al. *Proc. SPIE* (in press)
215. Kobayashi T (Ed.) *J-Aggregates* (Singapore: World Scientific, 1996)
216. Spano F C, Mukamel S *Phys. Rev. A* **40** 5783 (1989)
217. Knoester J *Phys. Rev. A* **47** 2083 (1993)
218. Bakalis L D, Knoester J *J. Luminescence* **87 – 89** 66 (2000)
219. Bakalis L D, Knoester J *J. Luminescence* **83 – 84** 115 (1999)
220. Ivanov A A et al. *Chem. Phys. Lett.* **418** 19 (2006)
221. Akimov D A, Siebert T, Kiefer W, Zheltikov A M *J. Opt. Soc. Am. B* (in press)